Palaeogeography, Palaeoclimatology, Palaeoecology 562 (2021) 110091

Contents lists available at ScienceDirect

Palaeogeography, Palaeoclimatology, Palaeoecology

journal homepage: www.elsevier.com/locate/palaeo

Pre-cenozoic evolution of the northern Qilian Orogen from zircon geochronology: Framework for early growth of the northern Tibetan Plateau

Bing Li [a,b,c], Andrew V. Zuza [c], Xuanhua Chen [a,b,*], Zeng-Zhen Wang [a,b], Zhaogang Shao [a,b], Drew A. Levy [c], Chen Wu [d], Shenglin Xu [a,b], Yujun Sun [a,b]

[a] Chinese Academy of Geological Sciences, Beijing 100037, China
[b] Sinoprobe Center, Chinese Academy of Geological Sciences and China Geological Survey, Beijing 100037, China
[c] Nevada Bureau of Mines and Geology, University of Nevada, Reno, Nevada 89557, USA
[d] Key laboratory of Continental Collision and Plateau Uplift, Institute of Tibetan Plateau Research, Center for Excellence in Tibetan Plateau Earth Sciences, Chinese Academy of Sciences, Beijing 100101, China

ARTICLE INFO

Keywords:
Orogenic plateau
U–Pb zircon dating
Tectonic history
Sediment provenance analysis
Basin development

ABSTRACT

The northern Qilian Shan, located along the northeastern margin of the Tibetan Plateau, experienced multiple phases of orogeny throughout the Phanerozoic, culminating in fold-thrust and strike-slip deformation associated with the Cenozoic India-Asia collision. Earlier phases of deformation in the Qilian Shan have been severely reactivated or transformed by the most recent Cenozoic strain. To better understand the tectonic evolution of this complex region, we conducted an integrated investigation of field observations, U–Pb dating of igneous and detrital zircons, and a synthesis of previously published data to constrain and reconstruct the pre-Cenozoic history of the northern Qilian Shan. This effort reveals five major age populations important to the history of this region: 2550–2350, 1850–1750, 1050–950, 500–435, and 320–240 Ma. Using this dataset, we identified three major depositional shifts and/or variations in drainage patterns that affected sediment provenance of the northern Qilian Orogen. Observed regional geologic constraints, the magmatic history, and new geophysical observations of the deep structure allow us to propose a coherent tectonic model for the pre-Cenozoic evolution of the northeastern margin of the Tibetan Plateau. (1) Late Neoproterozoic to Cambrian rifting opened the Qilian Ocean. (2) Early Cambrian subduction initiation along the margins of Qaidam and North China–Tarim continents resulted in Cambrian-Ordovician bivergent subduction, arc magmatism within these two continents, and consumption of the Qilian Ocean. (3) Final ocean closure and continental collision occurred at ca. 440 Ma and was associated with syn- and post-orogenic magmatism. (4) Collisional orogeny variably eroded the basement rocks, reorganized drainage networks, and altered sedimentary provenance for the lower Paleozoic to upper Paleozoic deposits. (5) Mesozoic extension led to the development of thick Jurassic–Cretaceous terrestrial basins. This pre-Cenozoic history resulted in preexisting weaknesses and/or low-friction detachment horizons that played a decisive role in controlling the pattern, distribution, and timing of Cenozoic deformation across the northern Tibetan Plateau.

1. Introduction

The Qilian Shan (Shan = Mountains in Chinese) tectonic belt, located along the northeastern margin of the Tibetan Plateau, marks the transitional zone between the Himalayan-Tibetan Orogen to the south and the North China Craton to the north (Fig. 1; e.g., Yin and Harrison, 2000; Heubeck, 2001; Yin et al., 2007a, 2007b; Stampfli et al., 2013; Zhu et al., 2013; Wu et al., 2016, 2017a; Zuza et al., 2018; Liu et al., 2018a, 2019). Although extensive studies had focused on the evolution of these two tectonic domains, relatively limited research has been devoted to investigating the tectonic history of their transitional boundary in the Qilian Shan, which is comprised of intervening oceanic and continental

* Corresponding author at: Chinese Academy of Geological Sciences, Beijing 100037, China.
E-mail addresses: libing@cags.ac.cn (B. Li), azuza@unr.edu (A.V. Zuza), xhchen@cags.ac.cn (X. Chen), wangzz@cags.ac.cn (Z.-Z. Wang), drewlevy@nevada.unr.edu (D.A. Levy), wuchen@itpcas.ac.cn (C. Wu), xushenglindizhi@163.com (S. Xu), sunyujunabc@163.com (Y. Sun).

https://doi.org/10.1016/j.palaeo.2020.110091
Received 23 April 2020; Received in revised form 9 October 2020; Accepted 13 October 2020
Available online 24 October 2020

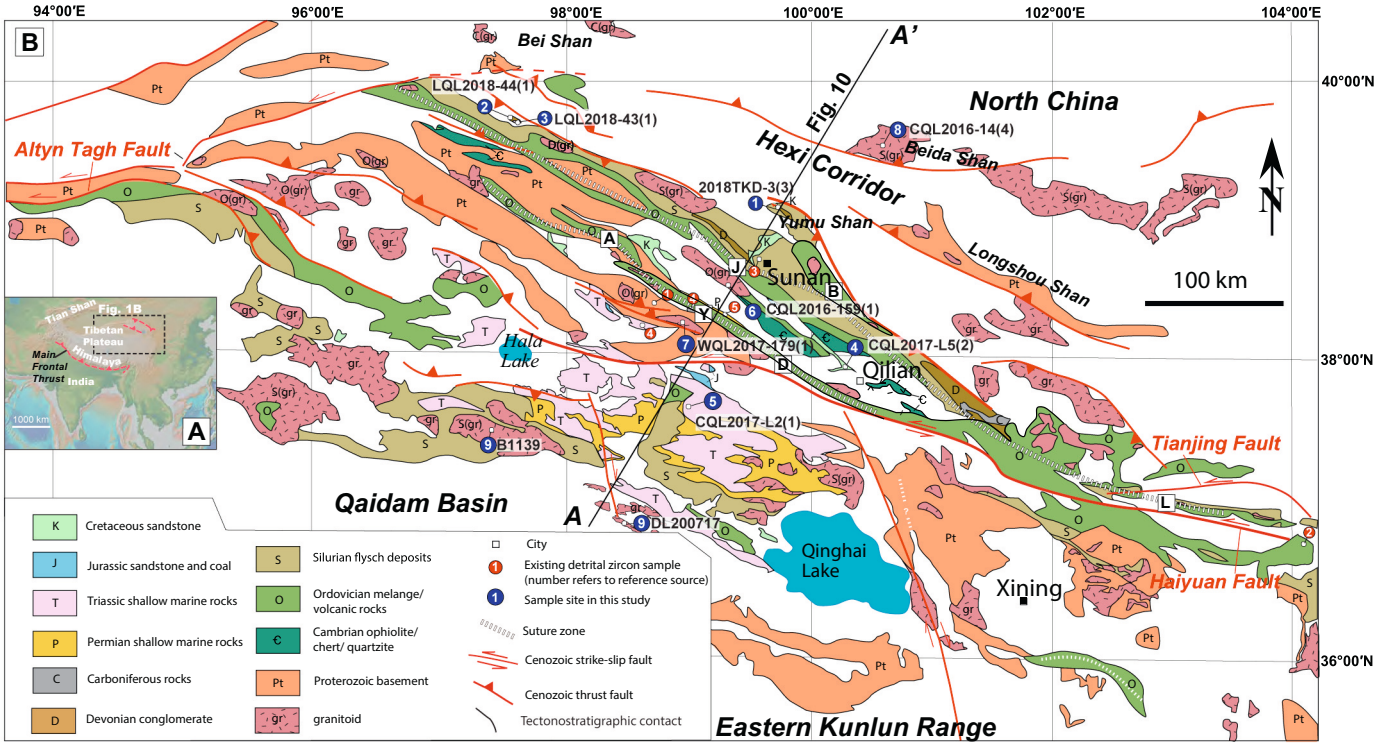

Fig. 1. Geologic map of the northern Tibetan Plateau (Modified form Wu et al., 2017a). Abbreviated early Paleozoic Qilian ophiolites (letters in square symbols): A–Aoyougou; B–Biandukou; D–Dongcaohe; J–Jiugequan; L–Laohushan; Y–Yushigou. Section line A–A′ corresponds to the deep structures based on the magnetotelluric (MT) method explored in Fig. 10. Existing data are from 1) Wu et al., 2017a; 2) Xu et al., 2010a; 3) Yang et al., 2009; 4) Zuza et al., 2018; 5) Song et al., 2019.

fragments (e.g., Yin et al., 2007a, 2007b; Xiao et al., 2009; Song et al., 2013; Wu et al., 2017a; Zuza et al., 2018; Liu et al., 2019). A major challenge in deciphering the origin and geologic history of the Qilian Shan is that the region experienced multiple phases of orogeny since the Neoproterozoic, and earlier tectonic features were severely overprinted or reactivated by the later phases of Mesozoic extension and Cenozoic crustal shortening (Yin and Harrison, 2000; Chen et al., 2003, 2004; Cowgill et al., 2003; Yin, 2010; Gao et al., 2013; Zuza et al., 2018, 2019; Li et al., 2020).

In particular, the early Paleozoic Qilian Orogen was a major tectonic event that involved ocean closure and collisional orogeny, and how the Qilian Orogen impacted the Cenozoic deformation history of the Tibetan Plateau is poorly resolved. This has in turn led to questions regarding the spatiotemporal framework of the early Paleozoic Qilian Orogen, including the initial timing of continental collision (e.g., Song et al., 2004; Wu et al., 2006; Tung et al., 2007; Lin et al., 2010; Wu et al., 2016), and age and distribution of the ophiolites suture zones (e.g., Song et al., 2013, 2014, 2019). There are multiple hypotheses for the polarity of subduction leading to the closure of the Neoproterozoic–early Paleozoic Qilian Ocean, including north-dipping, south-dipping, and bivergent subduction (e.g., Yin and Harrison, 2000; Yang et al., 2002; Wu et al., 2006; Gehrels et al., 2003a, 2003b, 2011; Yin et al., 2007a, 2007b; Xiao et al., 2009; Song et al., 2013, 2014; Xu et al., 2015; Zuza et al., 2018; Chen et al., 2019a; Liu et al., 2019). Improved understanding of this tectonic framework has led to a new appreciation of how these pre-Cenozoic structures influence Cenozoic intracontinental deformation in the northern Tibetan Plateau as part of the Himalayan-Tibetan orogen (Zuza et al., 2018; Li et al., 2019, 2020; Wu et al., 2019a; An et al., 2020; Bian et al., 2020). Favorably oriented crustal-scale preexisting weaknesses derived from the early Paleozoic Qilian subduction system and orogen may have caused deformation to initiate in the Qilian Shan shortly after the initial India-Asia collision in the Eocene (e.g., Allen et al., 2017; Zuza et al., 2018; Bian et al., 2020; Li et al., 2020). Earlier models for northern Tibet deformation considered Qilian Shan deformation to occur later, resulting from the expansion of a central plateau with high gravitational potential energy (e.g., England and Houseman, 1989; Molnar et al., 1993), possibly exploiting preexisting subduction systems (Tapponnier et al., 2001).

To better constrain the orogen, we conducted an integrated investigation of field observations, U–Pb dating of igneous and detrital zircons, and a synthesis of previously published data including the distribution of major suture zones, magmatism, and new geophysical observation of the deep structures across the Qilian Shan. Our new field and analytical observations allow us to reconstruct the pre-Cenozoic evolution of the northern Qilian Shan, and outline the influence on Cenozoic deformation in northern Tibet.

2. Geologic setting

The present-day triangular map-view pattern of the Qilian Shan, extending for >1000 km across the northeastern margin of the Tibetan Plateau (Fig. 1A), is bounded by the left-slip Altyn Tagh Fault to the west (e.g., Burchfiel et al., 1989; Meyer et al., 1998; Yin et al., 2002; Chen et al., 2003; Cowgill et al., 2000, 2003; Wu et al., 2019b), Qaidam Basin to the south (e.g., Wang et al., 2006; Yin et al., 2008a, 2008b; Cheng et al., 2015; Wu et al., 2019b; Zuza et al., 2019), and Hexi Corridor foreland to the northeast (Fig. 1B; Wang and Coward, 1993; Métivier et al., 1998; Bovet et al., 2009; Zuza et al., 2016). This NW-trending tectonic belt can be divided into the northern Qilian Orogenic Belt, central Qilian Terrane, and southern Qilian Terrane (Wu et al., 1993; Gehrels et al., 2003a; Yue et al., 2005; Bovet et al., 2009; Xiao et al., 2009; Wu et al., 2017a; Yan et al., 2019). The Qilian Shan is dominated by exposures of the early Paleozoic Qilian Orogen (Figs. 1B; Yin and Harrison, 2000; Yin et al., 2007a, 2007b; Song et al., 2013, 2014, 2017; Zuza et al., 2018; Liu et al., 2019). The original configuration of this orogen has since been transformed and overprinted by Mesozoic extension with a pulse of compressional strain in the early Cretaceous (e.g., Chen et al., 2019a) and Cenozoic multi-phase intracontinental deformation resulting from the India-Asia collision and continued convergence (e.g., Yin and Harrison, 2000; Jolivet et al., 2001; Qi et al., 2016; Zuza et al., 2019; Li et al., 2020).

2.1. Paleozoic orogen

The Qilian Orogen records the closure of the Qilian Ocean during the collision between Kunlun–Qaidam Terrane and the North China Craton (Şengör and Natal'in, 1996; Sobel and Arnaud, 1999; Yin and Harrison, 2000; Gehrels et al., 2003a, 2003b; Yin et al., 2007a, 2007b; Xiao et al., 2009; Wu et al., 2016; Zuza et al., 2018; Chen et al., 2019a). The orogen is composed of early Paleozoic ophiolitic mélange, Ordovician–Silurian granitoid plutons and arc belts, Silurian flysch sequences, Devonian molasse, and Carboniferous to Permian sedimentary rocks. The ophiolite mélange, commonly referred to as the North and South Qilian suture zones (Fig. 1B; e.g. Song et al., 2013, 2017; Xiao et al., 2009; Xia et al., 2012), is evidence for the existence of the Neoproterozoic–Ordovician Qilian Ocean between Qaidam and North China (e.g., Tseng et al., 2007; Xia and Song, 2010; Song et al., 2013, 2014, 2017, 2019; Li et al., 2017; Zuza et al., 2018). Continued oceanic subduction and related arc magmatism led to the convergence of these terranes (Qian et al., 1998; Cowgill et al., 2003; Gehrels et al., 2003a; Shi et al., 2004; Wu et al., 2004, 2006, 2010; Hu et al., 2005; Quan et al., 2006; He et al., 2007; Tseng et al., 2009; Dang, 2011; Xia et al., 2012; Xiong et al., 2012; Song et al., 2013, Huang et al., 2015; Zuza et al., 2018), which resulted in the formation of the fragmented Qilian suture zones during the collision (Fig. 1B). The orogen probably involved prolonged intracontinental deformation after Late Ordovician–Early Silurian ocean closure (e.g., Song et al., 2004, 2006; Lin et al., 2010).

2.2. Mesozoic extension

The northern Tibetan Plateau, including the Qilian Shan, underwent Mesozoic regional extension or transtension, which led to the deposition of Jurassic–Cretaceous terrestrial strata (Chen et al., 2003, 2004, 2019a; Yin et al., 2008a, 2008b; He et al., 2019; Shao et al., 2019; Zuza et al., 2019). This phase of deformation was possibly triggered by the far-field effects of subduction and closure of the Paleo-Tethys Ocean along the Kunlun-Anyemaqen suture zone (e.g., Cheng et al., 2019a). Limited extensional structures have been directly observed across the Qilian Shan (e.g., Shao et al., 2019; Zuza et al., 2019), possibly suggesting most of the Mesozoic tectonic features have been reactivated and/or overprinted by the subsequent contractional deformation since early Cenozoic (Cheng et al., 2019a, 2019b; Zuza et al., 2019; An et al., 2020; Li et al., 2020). This region may have also experienced a local pulse of early Cretaceous contractional strain, resulting in the development of Cretaceous folds and thrusts in Yumu Shan, in the northern Qilian Shan, supported by geologic mapping and seismic profile interpretation (Chen et al., 2019b). This phase of deformation is important for the history of the Qilian Shan but is poorly understood at present.

2.3. Cenozoic deformation

The Cenozoic Qilian Shan thrust belt is comprised of thrust and strike-slip faults, which help accommodate India-Asia convergence along the northeast margin of the Tibetan Plateau (Tapponnier et al., 2001; Duvall et al., 2013; Yuan et al., 2013; Yin et al., 2008a, 2008b; Zuza and Yin, 2016; Li et al., 2019). Cenozoic deformation appears to have propagated to northern Tibet by 50–40 Ma (e.g., Jolivet et al., 2001; Clark et al., 2010; He et al., 2018; Cheng et al., 2016a; An et al., 2020; Li et al., 2020) involving thrust-related deformation, followed by a pulse of deformation starting at 20–15 Ma. This second phase of deformation resulted in the development of major thrust and strike-slip fault systems, including Haiyuan and Kunlun left-slip faults (Fig. 1B; e.

g., Duvall et al., 2013; Zheng et al., 2017; Li et al., 2019; Yu et al., 2019; Wang et al., 2020a), which led to rapid mid-Miocene regional exhumation, crustal shortening, and the formation of a major geomorphic boundary between the northern Tibetan Plateau and its northern foreland.

2.4. Stratigraphy and sediment characteristics

The study area is mainly located in the northern Qilian Shan and includes the Yumu Shan in the north (~38–39°N, ~98–100°E; Fig. 1B). Sub-parallel early Paleozoic suture belts and Cenozoic thrust faults constitute significant parts of the NW-trending Qilian Shan. Older Proterozoic to Mesozoic rocks were thrusted over younger Mesozoic and Cenozoic strata. Below we describe the major stratigraphy and sediment characteristics (Fig. 2).

Sedimentary rocks with ages ranging from Ordovician to Quaternary are exposed throughout the northern Qilian Shan (Fig. 1B). Ordovician rocks consist of low-grade metamorphosed and strongly deformed sandstone, siltstone, and limestone with minor volcanic rocks (Figs. 2 and 3A), which probably represent a complex tectonic mingling of forearc, accretionary wedge, and foreland-basin strata (e.g., Xiao et al., 2009). Silurian strata consist of deformed turbidite sequences with interfingering conglomerate beds (Figs. 2 and 3B), which are interpreted

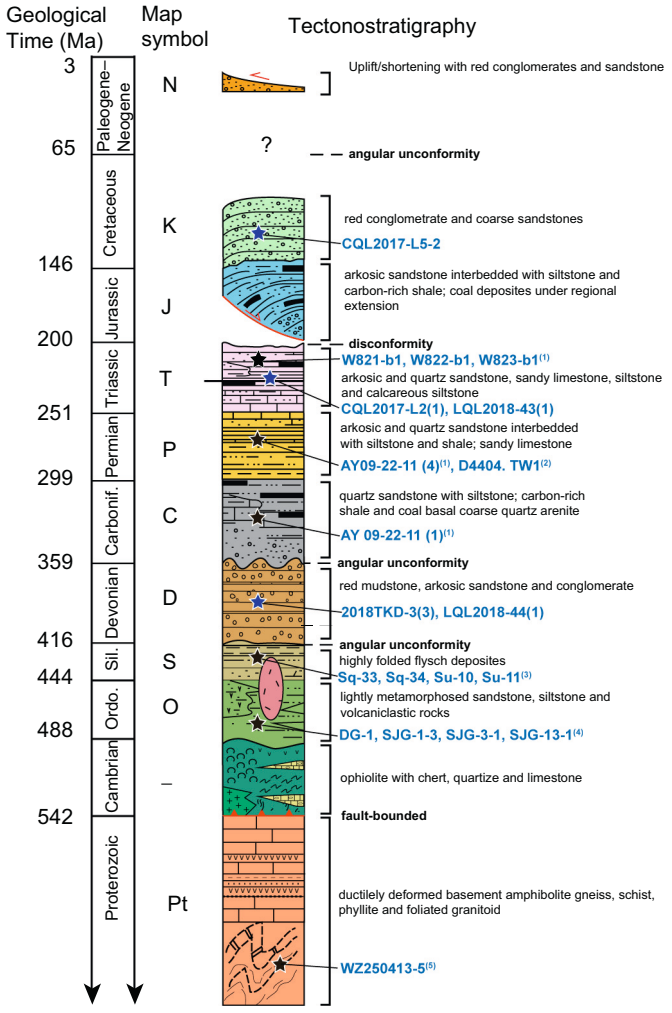

Fig. 2. Tectonostratigraphy of the northern Qilian Shan. Also shown are U–Pb detrital zircon samples of major strata (blue stars from this study; black stars from 1) Zuza et al., 2018; 2) Song et al., 2019; 3) Yang et al., 2009; 4) Xu et al., 2010a; 5) Wu et al., 2017a. (For interpretation of the references to color in this figure legend, the reader is referred to the web version of this article.)

to represent a flysch basin that transitions into molasses deposits (Du et al., 2003). Devonian strata consist of epicontinental deposits of pebble conglomerate, sandstone, mudstone, and minor volcanic rocks (Figs. 3C–D). These sediments are interpreted as molasse deposited in intermontane and/or foreland basins during the Qilian Orogeny (Yan et al., 2007; Xu et al., 2010b; Xia et al., 2012; Song et al., 2013). Carboniferous strata, composed of conglomerate, quartz arenite, arkosic sandstone, and siltstone, with minor carbon-rich shale and coal, unconformably overlie the Ordovician–Devonian rocks and metamorphic rocks. The Permian rocks consist of limestone, coarse sandstone, and interbedded siltstone.

Triassic strata, consisting of interbedded limestone, arkosic sandstone, siltstone, and shale (Fig. 3E), conformably overlie Permian rocks. The lithology of Jurassic strata consists of interbedded quartz arenite, siltstone, and coal-bearing shale (Fig. 2), which conformably overlie upper Triassic sequences. The Cretaceous strata are composed of conglomerate and quartz arenite. They exhibit growth strata geometry in the northern Qilian Shan (Fig. 3F) and might have been deposited in extensional grabens or rift basins (Yin et al., 2008b).

Neoproterozoic and early Paleozoic plutons are exposed throughout the Qilian Shan (Fig. 1B; e.g., Gehrels et al., 2003a, 2011; Yin et al., 2007a, 2007b; Chen et al., 2012; Song et al., 2013; Huang et al., 2015; Wu et al., 2017a, 2017b; Zuza et al., 2018; Liu et al., 2019). Neoproterozoic plutons consist of earlier arc-related granitoids (e.g., Tung et al., 2012, 2013; Wu et al., 2017a; Liu et al., 2018b) and subsequent A-type granitoids that may have originated during post-collision continental rifting (e.g., Tung et al., 2013; Wu et al., 2017a). These plutons intruded into the older Proterozoic metamorphic basement. The early Paleozoic plutons, ranging in composition from alkali feldspar leucogranite to syenite to quartz monzonite, are attributed to Cambrian-middle Ordovician subduction-related and/or late Ordovician–early Devonian syn-collisional to post-collisional magmatism with ages spanning 516 to 374 Ma (e.g., Gehrels et al., 2003a; Tseng et al., 2009; Huang et al., 2015; Zuza et al., 2018; Liu et al., 2019; Wang et al., 2020b). These plutons intruded the Proterozoic gneiss and schist complex and sometimes Ordovician strata (Fig. 2), and are overlain by Carboniferous and younger strata (Zuza et al., 2018).

3. Geochronology methods

Zircon grains were separated from whole-rock samples (about 4–6 kg) by standard methods in the Hebei Institute of Geology and Mineral Resources in China. Zircon crystals were randomly selected, mounted in epoxy resin with zircon standards for U–Pb analysis by laser ablation-inductively coupled plasma-mass spectrometry (LA–ICP–MS). Cathodoluminescence (CL) images were collected to identify the internal texture of the zircon grains and guide age interpretation (Fig. 4). Most zircons of these samples were analyzed on the Thermo Fisher Ltd. Neptune multiple-collector ICP–MS with ESI Ltd. New Wave 193 nm FX ArFexcimer LA system at the Isotopic Laboratory, Tianjin Institute of Geology and Mineral Resources of China Geological Survey following the procedures described of Geng et al. (2011). One sample (i.e., DL200717) was analyzed by LA–ICP–MS at the University of Texas at Austin UTChron laboratory using a PhotonMachine Analyte G.2 excimer laser with a large-volume Helex sample cell and a Thermo Element2 ICP–MS. The detailed analytical methods employed for analyses are described in Gehrels et al. (2011).

For igneous rocks, the goal in U–Pb zircon dating was to determine their crystallization ages. We analyzed approximately 20–30 zircon gains from each sample and examined the age distribution of concordant analyses (Fig. 5). In general, the primary population of younger ages was interpreted as the crystallization age, and older grains were attributed to grain inheritance. For rare samples with a distinct individual young analysis, we either did not consider them further if they were discordant or attributed them to Pb loss due to a subsequent metamorphic and/or reheating event. Older zircon ages were attributed to grain inheritance.

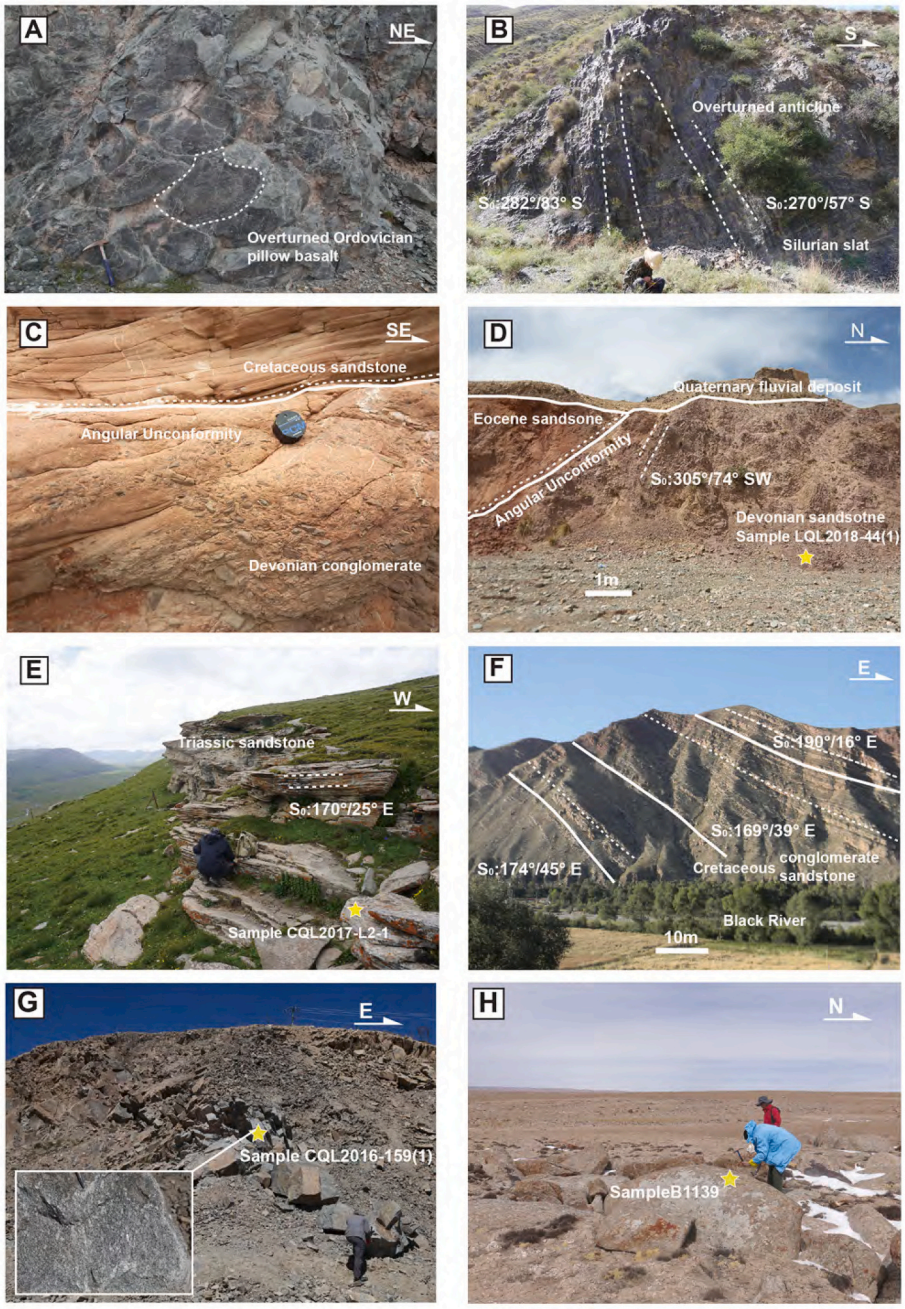

Fig. 3. Field photographs from the Qilian Shan displaying important geologic relationships. (A) Outcrop of overturned Ordovician pillow basalt exposed in the northern Qilian Shan. (B) Outcrop of south-dipping overturned Silurian slate from the Yumu Shan, north of Qilian Shan. (C) Angular unconformity between the Cretaceous strata and underlying Devonian strata exposed in the Yumu Shan. (D) Depositional contact between the Devonian strata and Eocene strata along the northern margin of the northern Qilian Shan. The sandstone sample LQL2018-44(1) from Devonian strata is indicated. (E) Outcrop of the east-dipping Triassic sandstone and sample CQL2017-L2-1. (F) Growth strata of Cretaceous strata along the Black River north of Qilian Country. (G-H) Outcrop of the granitoids samples CQL2016-159(1) and B1139. Note the attitudes reported in the figures are in the form of strike and dip.

The concordia diagrams and weighted mean ages were calculated and plotted using Isoplot 3.0 (Ludwig, 2003). For detrital zircon U–Pb dating, we aimed to determine sediment provenance and reconstruct the tectonic setting on a regional scale (e.g., Fedo et al., 2003; Cawood et al., 2012). Approximately 100 zircon grains were analyzed for each sandstone sample. The cumulative distribution diagram and normalized probability density plots (Fig. 6) of detrital zircon samples were calculated and plotted by detritalPy by Sharman et al. (2018).

The reported ages for zircon analyses (i.e. best age) were determined from the $^{206}Pb/^{238}U$ for analyses with an age younger than 1000 Ma and from $^{207}Pb/^{206}Pb$ for analyses with an age older than 1000 Ma (e.g., Gehrels et al., 2011). Reported uncertainties including measurement errors for age determination of individual grains are at the 1σ level. To determine the crystallization ages for the igneous rocks, only examined analyses with discordance of <10% are considered. We focused on the dominant signatures of younger analyses and interpreted the weighted mean age of the youngest cluster as the sample's crystallization age (e.g., Davis, 1997). For detrital zircon data, analyses with <30% discordance or >5% reverse discordance are considered (e.g., Gehrels et al., 2011). The geochronologic age data for each sample with errors and related raw data are presented in the Supplementary material.

4. Sample descriptions and results

Five granitoid samples and five sandstone samples were collected across the Qilian Shan and adjacent areas. Detailed sample locations and lithology are listed in Table 1 and also shown in Figs. 1B and 2.

4.1. U–Pb zircon geochronology of granitoids

Five granitoid samples were analyzed, including four granite samples and one granodiorite sample (Table 1). U–Pb concordia diagrams

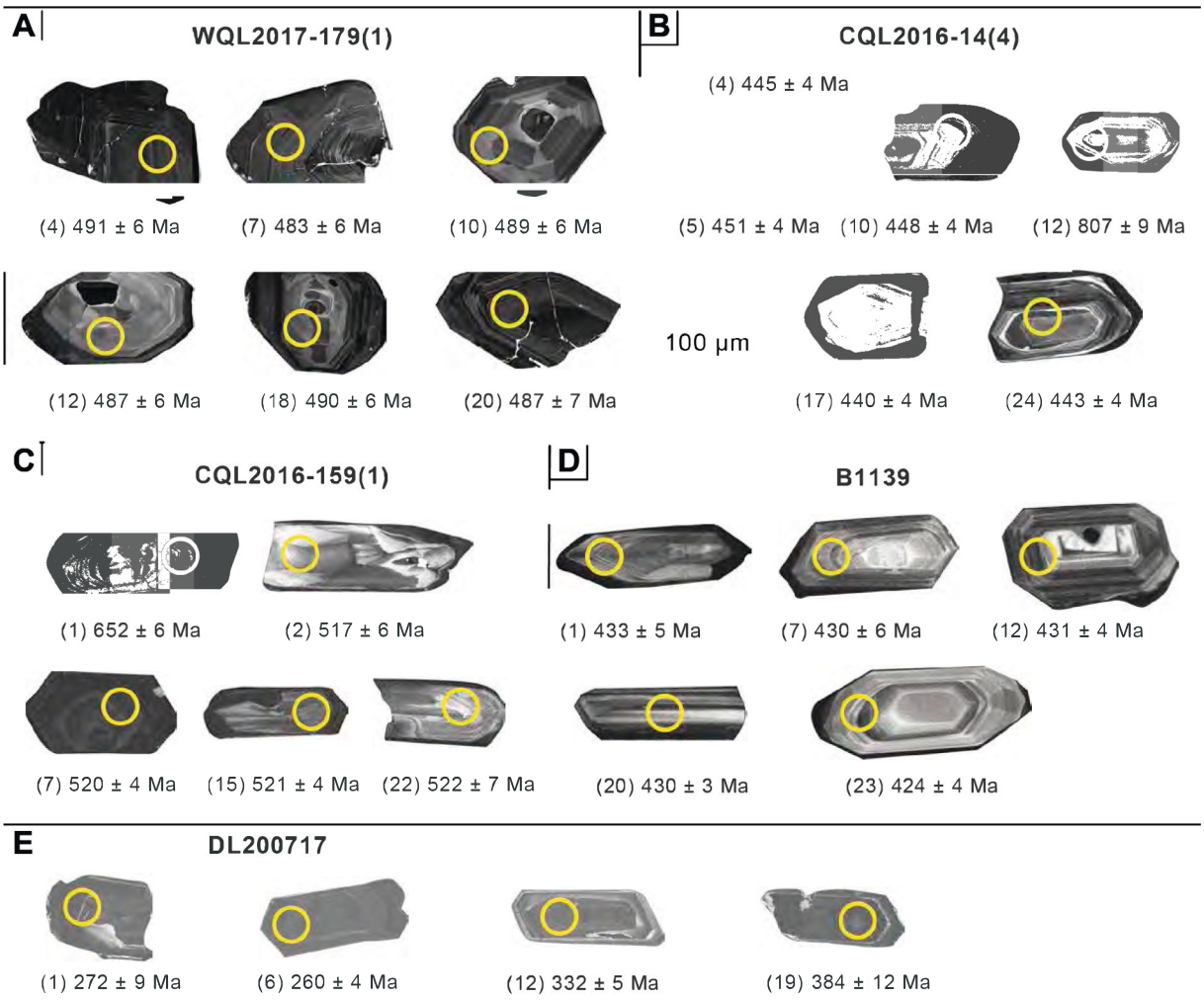

Fig. 4. Representative cathodoluminescence (CL) images of zircon dated from granitic rock in this study. Yellow circles are analyzed spots for U–Pb dating. Scale bar in B applies to all panels. (For interpretation of the references to color in this figure legend, the reader is referred to the web version of this article.)

showing the results of single-shot zircon analyses, weighted mean age calculation, and interpreted crystallization ages for each sample are showed in Fig. 5 and Supplemental file Table S1.

In previous studies, most of the exposed plutonic rocks throughout the Qilian Shan were inferred to be early Paleozoic in age (Fig. 1B; e.g., Pan et al., 2004; Wu et al., 2010; Song et al., 2013; Wu et al., 2016, 2017a; Liu et al., 2019). We analyzed five of these granitoids to constrain the timing of local magmatism associated with the Qilian Orogen. Sample CQL2016-159(1) was collected from the Zoulang Nan Shan pluton, one of the largest plutonic bodies in the northern Qilian Shan (Figs. 1B and 3G). Twenty-five zircon grains were analyzed, and U–Pb ages range from 492 to 1517 Ma. Th/U ratios of this sample range from 0.09–0.70. The weighted average of 11 concordant analyses is 520 ± 3 Ma (mean square of weighted deviates [MSWD] = 0.6; Fig. 5A). The other analyses were excluded because of discordance and/or low radiogenic Pb.

Sample WQL2017-179(1) is a granite collected from the central Qilian Shan (Fig. 1). Twenty-five zircons were analyzed with U–Pb ages ranging from 396 to 584 Ma. Th/U ratios of the sample range from 0.40–0.75. The weighted mean age of concordant analyses (n = 16) is 229 ± 2 Ma (MSWD = 1.9; Fig. 5B).

Granodiorite sample CQL2016-14(4) was collected in Beida Shan, north of Hexi Corridor (Fig. 1B). Twenty-five zircons were analyzed, yielding diverse U–Pb ages ranging from 440 to 1100 Ma, with Th/U ratios ranging from 0.10 to 0.85. The weighted mean U–Pb age of 14 concordant analyses is 444 ± 2 Ma (MSWD = 0.8; Fig. 5C).

Sample B1139 was collected from an undeformed monzonitic granite located ca. 80 km south of Hala Lake, in the southern Qilian Shan (Figs. 1B). The pluton intrudes into the Silurian unit, and it was denude-planned by the subsequent early Cenozoic deformation (Fig. 3H; Jia et al., 2018). Twenty-nine grains were analyzed, and U–Pb ages range from 424 to 751 Ma. The Th/U ratios of this sample range from 0.16 to 1.06. Twenty-one concordant ages define the best age population, and the weighted mean of these ages is 430 ± 1 Ma (MSWD = 1.3; Fig. 5D).

Granite sample DL200717 was collected from north of the Buguote Shan, north of Qaidam basin (Fig. 1B). We analyzed 21 zircons, and most were high-U zircons (>500 ppm U). Of these analyses, 13 analyses gave concordant U–Pb ages that ranged from 129 to 273 Ma, with Th/U ratios ranging from 0.31 to 1.14. Spot 3 yielded a distinct younger age (129 Ma; Table S1). The other youngest population of 12 analyses yielded a weighted mean age of 253 ± 7 Ma (MSWD = 38), which is interpreted as the crystallization age of this granite sample (Fig. 5E). We note that this sample may have experienced metamictization, evidenced by the high U and pervasive discordance, which may explain the unusually high MSWD value. Therefore, we acknowledge that this Permian–Triassic age should be treated with caution. However, the tight cluster of analyses at ca. 250 Ma (Fig. 5E) suggests that this age may be significant since similar pluton ages have been found along strike (e.g., Wu et al., 2016).

4.2. U–Pb detrital zircon geochronology

Five sandstone samples were collected to fill in gaps in regional

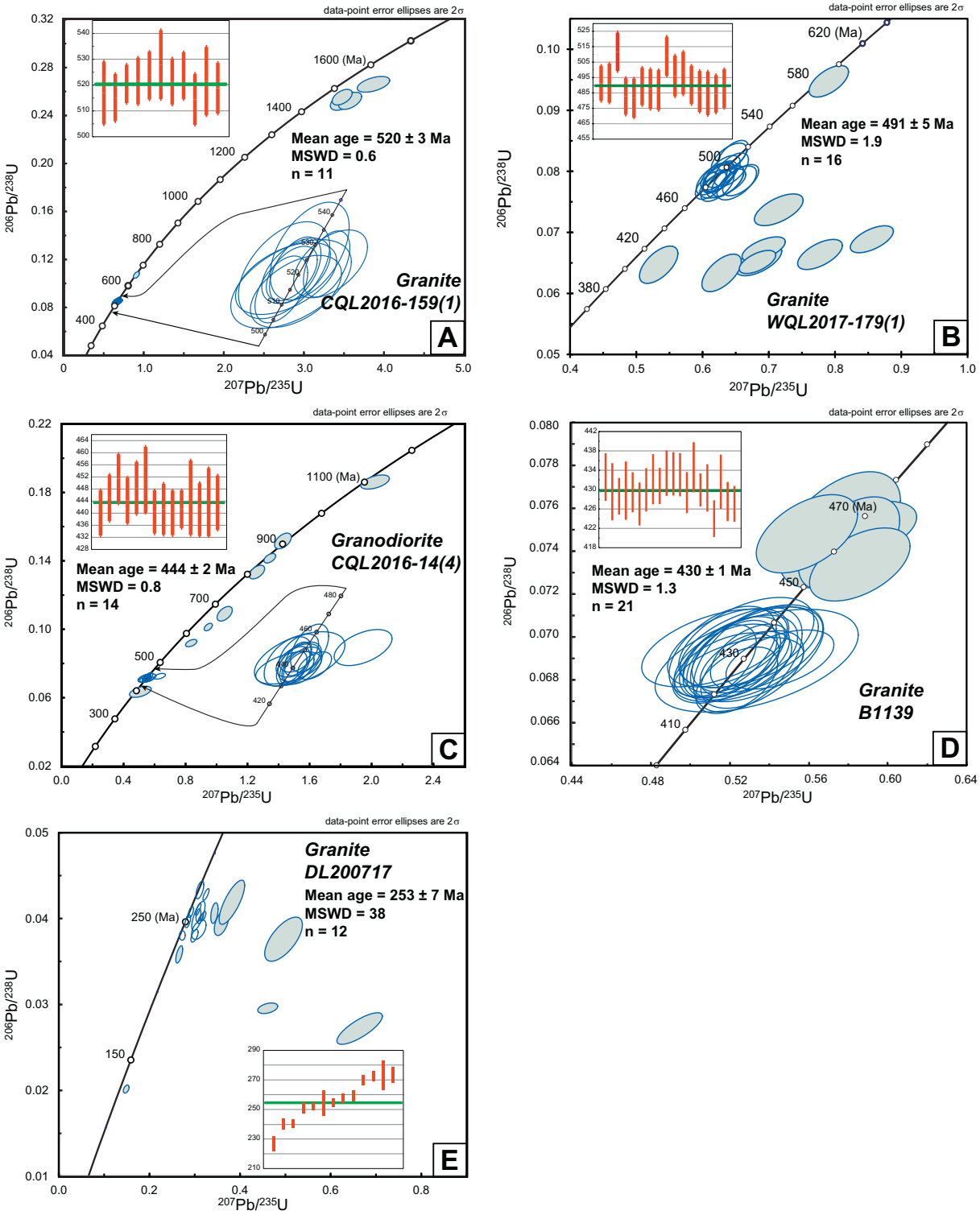

Fig. 5. U–Pb concordia diagrams showing results of single-shot zircon analyses and weighted mean age of zircon ages for granitic rock samples. All weighted mean ages are U–Pb ages at the 95% confidence level and only concordant ages are calculated in the calculation. Error ellipses are 2σ, and gray shaded ellipses show individual analyses that were excluded. MSWD–mean square of weighted deviates.

coverage of detrital zircon data from Devonian to Cretaceous strata in the northern Qilian Orogen (Fig. 2). The integrated dataset spans Neoproterozoic to Cretaceous strata, which allows the characterization of sediment provenance during the Pre-Cenozoic evolution of the Qilian Orogen. The results are presented as zircon U–Pb concordia plots and normalized relative probability plots in Fig. 6 and Supplementary Table S2, respectively. To further characterize zircon provenance, we use zircon Th/U ratios to constrain whether the grains are magmatic (Th/U > 0.1) or metamorphic (Th/U < 0.1) in origin (e.g., Belousova et al., 2002; Rubatto, 2002; Cheng et al., 2019c). Analyzed zircon age vs. Th/U ratios are showed in Fig. 7, indicating the predominant magmatic origin of all the analyzed samples.

The two Devonian sandstone samples (2018TKD-3(3) and LQL2018-44(1)) suggest distinct zircon ages distributions (Figs. 6A–B and 7D–E).

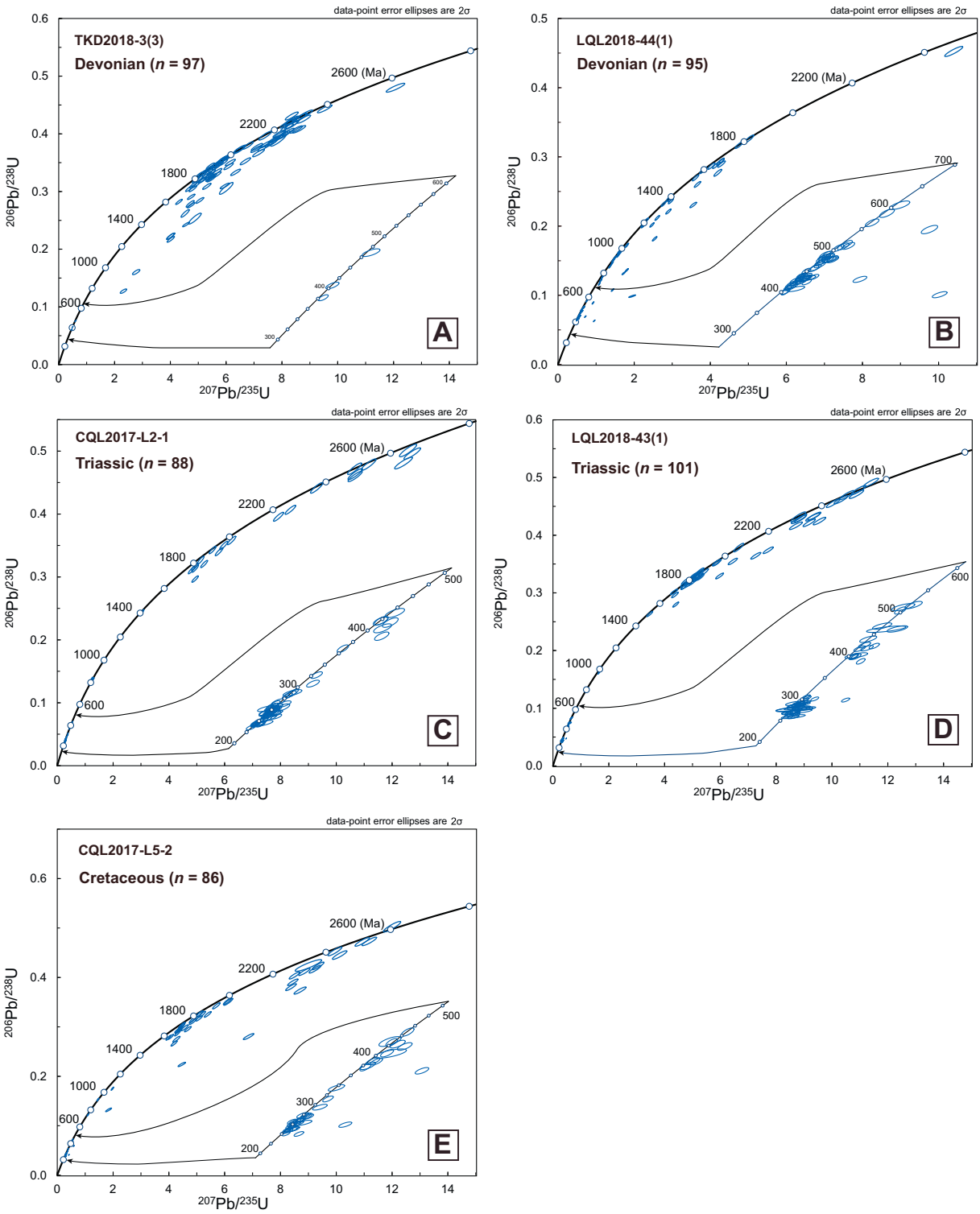

Fig. 6. U–Pb Concordia plots for detrital zircon grains of each sample.

Sample 2018TKD-3(3) is dominated by two Paleoproterozoic aged peaks at ca. 1950 and ca. 2272 Ma, with a smaller population at ca. 450–500 Ma. Zircon ages of sample LQL2018-44(1) are Cambrian-Devonian, primarily clustered at 400–520 Ma with two peaks at 431 and 480 Ma. Numerous minor age populations extend from the Neoproterozoic to Paleoproterozoic (Fig. 7D–E). The Th/U ratios of sample 2018TKD-3 (3) range from 0.14 to 1.87, with three exceptions of 0.03 (1838 Ma), 0.04 (1925 Ma) and 0.09 (1957 Ma) and the Th/U ratios of sample LQL2018-44(1) range from 0.13 to 1.74, with a single exception of 0.06 (1211 Ma) (Fig. 7D–E). The high Th/U ratios indicate a magmatic source for the Devonian samples.

The two Triassic arkosic arenite samples (CQL2017-L2-1 and LQL2018-43(1)) suggest similar zircon age distributions (Figs. 6C–D). Mesozoic-dominated zircon-age signatures were observed in these samples of CQL2017-L2-1 and LQL2018-43(1): 240–500 Ma, with peaks at ca. 256 and ca. 278 Ma, respectively. Minor Paleoproterozoic age populations are also present. Several grains yielded > 2.5 Ga Archean ages. Sample CQL2017-L2(1) yielded five ca. 225–235 Ma ages from

Table 1
Summary of U–Pb zircon geochronology samples in this study

Sample	Latitude (N) (°N)	Longitude (E) (°E)	Elevation (m) (m)	Age[a]	Lithology
Zircon geochronology samples of granitoids					
CQL2016-159(1)	38°38′24.50″	99°20′13.61″	3496	520 ± 3 Ma	Granite
WQL2017-179(1)	38°21′05.46″	99°21′41.42″	3525	491 ± 5 Ma	Granite
CQL2016-14(4)	39°38′57.00″	100°41′09.66″	1567	444 ± 2 Ma	Granodiorite
B1139	37°48′18.90″	97°22′37.20″	4371	430 ± 1 Ma	Granite
DL200717	37°08′41.50″	98°27′45.40″	3711	253 ± 7 Ma	Granite
Detrital zircon geochronology samples of sedimentary rocks					
2018TKD-3(3)	38°42′26.00″	98°38′59.50″	3589	Devonian	Quartz arenite
LQL2018-44(1)	39°41′18.70″	97°43′39.40″	2570	Devonian	Arkosic arenite
CQL2017-L2-1	37°53′51.54″	99°02′03.00″	4384	Triassic	Arkosic arenite
LQL2018-43(1)	39°41′15.70″	97°43′55.50″	2585	Triassic	Arkosic arenite
CQL2017-L5-2	38°12′50.70″	100°08′55.80″	2791	Cretaceous	Quartz arenite

[a] Interpreted U–Pb age for igneous samples and reported stratigraphic age of samples from sedimentary rocks. Reported uncertainties of the zircon U–Pb ages are at the 1σ level.

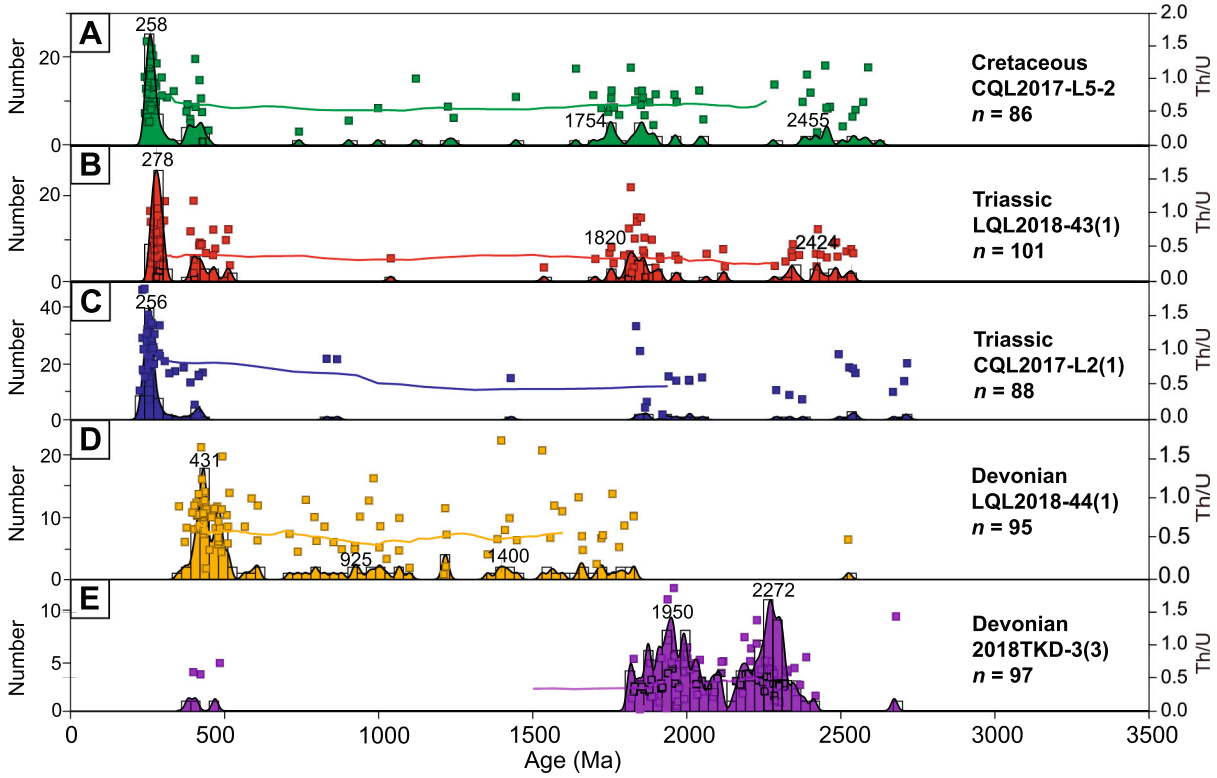

Fig. 7. Normalized relative probability plots of detrital zircon U–Pb ages and Th/U ratios for the five samples across the northern Qilian Orogen analyzed in this study.

single zircon grain, which may indicate a maximum depositional age of Late Triassic time (e.g., Dickinson and Gehrels, 2009; Supplemental file Table S1). The Th/U ratios of sample LQL2018-43(1) range from 0.12 to 1.38, with four exceptions of 0.04 (1809 Ma), 0.05 (402 Ma), 0.06 (1865 Ma) and 0.06 (277Ma). The Th/U ratios of CQL2017-L2-1 range from 0.18 to 3.46, with two exceptions of 0.02 (1922 Ma) and 0.07 (413 Ma). The Th/U ratios of both of the Triassic sandstones indicate magma-derived zircons (Figs. 7B–C).

The dominant zircon age population of the Cretaceous lithic quartz arenite sample CQL2017-L5-2 is at 240–460 Ma with a major peak at ca. 258 Ma. Two other significant populations lie at 1700–1900 Ma (1754 Ma peak) and 2250–2500 Ma (broad peak centered at ca. 2455 Ma). Minor age populations exist between 700 and 1500 Ma (Fig. 6E). The Th/U ratios range from 0.17 to 2.54, with one exception of 0.03 (428 Ma), suggesting a predominantly magmatic origin of the zircon grains (Fig. 7A).

5. Discussion

5.1. Sediment provenance analysis and tectonic setting of the northern Qilian Orogen

We interpret sedimentary provenance and tectonic setting based on our field observations (e.g., Fig. 3), new U–Pb detrital zircon dating of relevant strata and igneous rocks, and published age constraints from igneous rocks and detrital zircon data. We identified depositional shifts involving multiple source regions and variations in drainage patterns dictated in sediment provenance based on major changes in geochronology spectra. The relationship between depositional age and detrital zircon age populations can be used to infer the tectonic setting as discussed in Cawood et al. (2012).

A Meso-Neoproterozoic schist sample of the Tuolai group from central Qilian Shan shows three prominent zircon populations with

peaks at ca. 2480, ca. 1700, and ca. 1440 Ma (Wu et al., 2017a). These dominant age signatures are significantly older than the depositional age of the Tuolai Group–constrained to be between 1200 and 960 Ma based on maximum depositional ages and crosscutting intrusion, respectively (e.g., Wu et al., 2017a)–as cumulative distribution plots demonstrate (Fig. 8A). This zircon distribution supports an extensional setting for the rocks in the classification of Cawood et al. (2012), as the dominate zircon ages are much older than the time of sediment accumulation (Fig. 8A) and less than 1% of grains have ages within 150 Ma of the depositional age (Wu et al., 2017a; Table S2). Furthermore, when considered with similar analyzed rocks in the Qilian Shan, the Tuolai Group is intruded by ca. 1000–900 Ma arc granites (e.g., Wu et al., 2017a), which suggests that it was near the margins of the Proterozoic continent to be intruded by a Neoproterozoic arc system. Therefore, our observations support previous assertions that the Tuolai Group strata represent a southern passive margin of the contiguous North Tarim–North China Craton (Fig. 9A; Gehrels et al., 2003a; Tung et al., 2007; Wu et al., 2017a), which was subsequently intruded by ca. 1000–900 Ma magmatism, potentially during the closure of the Tarim Ocean (Fig. 9B; Guo et al., 2005; Wu et al., 2016, 2017a, 2017b; Zuza and Yin, 2017).

The Ordovician–Silurian samples exhibit similar age populations with three peaks at ca. 2500, ca. 1000, and ca. 450 Ma (Figs. 8G–H; Yang et al., 2009; Xu et al., 2010a). Detrital zircon age spectra and pie charts show that roughly 1/3 of the analyzed grains are very close in age to the depositional age of the strata, with subordinate amounts of early Neoproterozoic and Mesoproterozoic (Fig. 8G–H). With the dominance of early Paleozoic ages coupled with variable percentages of pre-Phanerozoic basement ages, we interpret that these strata were deposited within a collisional setting, but not necessarily a forearc basin, related to the early Paleozoic Qilian Orogen (Figs. 8A and 9E; Cawood et al., 2012; Zuza et al., 2018). Collision-induced shortening exhumed and eroded basement rocks with ca. 2.5 and ca. 1.0 Ga intrusions that were deposited in the Ordovician–Silurian samples.

The two analyzed Devonian sandstone samples displayed very different zircon age spectra. Sample LQL2018-44(1) shows a series of age groups ranging from Paleoproterozoic to Silurian, whereas sample 2018TKD-3(3) is dominated by two Paleoproterozoic aged peaks (Figs. 7D–E). For comparison, Devonian sandstone sample Shl 25-1 from the Laojun Shan Formation (Xu et al., 2010b) and sample AY 09-26-11 (12) from Zuza et al. (2018) in the northern Qilian Shan are comprised of mostly Ordovician and Silurian age clusters. Devonian strata in the Qilian Shan mainly consist of sub-angular, poorly-sorted terrestrial conglomerates (Fig. 3C) and sandstones (Fig. 3D) that were deposited in proximal molasse deposits of an intermontane or foreland basins (Xu et al., 2010b; Song et al., 2013). Sample 2018TKD-3(3) from Yumu Shan, with primarily Paleoproterozoic age signatures and only minor early Paleozoic zircons, was probably deposited near the uplifted Longshou Shan area, southern margin of North China Craton (Fig. 1B). The other Devonian sample, LQL2018-44(1), shows a variable age distribution with a unimodal 431 Ma zircon population and lesser Proterozoic age signals. The minor Proterozoic signal may have been influenced by the eroded Mesoproterozoic–Neoproterozoic strata.

These observations of dramatically distinct age distributions from different Devonian samples (Figs. 7D–E) demonstrate that they had variable drainage systems and source regions. These samples were probably deposited in disconnected basins with disparate sedimentary environments (i.e., facies), as part of a syn-to-post-collisional framework (Figs. 3 and 7D–E; Xu et al., 2010b; Zuza et al., 2018). None of the Devonian samples, including those from Xu et al. (2010b) and Zuza et al. (2018), yielded a dominant population of grains older than ca. 2500 Ma. Sample LQL2018-44(1) yielded essentially no grains older than ca. 1800 Ma, compared to Silurian and older rocks that were comprised of an appreciable percentage of Archean grains (Figs. 8G-I). Therefore, we take the Silurian to Devonian transition as the first provenance shift observed in this study, where Devonian samples have variable proximal sources that do not include Archean grains. The Late Neoarchean zircon grains from older samples were likely derived from the distant interior of the North China craton (e.g., Zhao et al., 2002a), whereas the early Paleoproterozoic grains were probably from a local source along the southern margin of the North China Craton in the Longshou Shan (e.g., Gong et al., 2011) or other comparable basement exposures.

The Carboniferous sample from the central Qilian Shan shows a predominately unimodal peak of 450–500 Ma ages (Fig. 8E; Zuza et al., 2018). This age spectrum demonstrates the second provenance shift from a significant Mesoproterozoic-Neoproterozoic zircon component to mostly early Paleozoic ages, transitioning from Devonian to Carboniferous strata. This pattern also suggests that its source area is local within Qilian Orogen as indicated by the Qilian arc zircon ages (e.g., Zuza et al., 2018; Liu et al., 2019; this study). There must have been a drainage system eroding either the arc rocks associated with the Qilian Orogen and/or the forearc sediments from the same Qilian Orogen-source region during the continuous process of sediment recycling, rather than Mesoproterozoic–Neoproterozoic basement.

The Permian to Cretaceous samples (Zuza et al., 2018; Song et al., 2019b; this study) show four similar age peaks of 2500, 1800, 450, and 300 Ma, with increasing Permian-Triassic zircon populations and decreasing early Paleozoic zircons through time. We infer that these strata were deposited in Mesozoic intracratonic basin settings across the Qilian Shan, as revealed by the cumulative distribution plot in Fig. 8A. The transition from Carboniferous to Permian strata represents the third provenance shift, with dominant nearly unimodal early Paleozoic zircon populations giving way to more diverse grains from the Proterozoic basement and Permian-Triassic igneous rocks. Our dated Triassic granite (sample DL200717) demonstrates the existence of local Permian–-Triassic granites in the Qilian Shan, as also recognized by Wu et al. (2016). The emergence and predominance of Permian-Triassic zircon grains since the Permian in the Qilian Orogen suggest these strata have contributions from either (1) localized sources and zircon grains ultimately derived within the orogen (Fig. 5E; e.g., Chen et al., 2012; Wu et al., 2016) or (2) distant sources such as the Eastern Kunlun Range to the south across Qaidam Basin (e.g., Pullen et al., 2008; Cheng et al., 2016b; Wu et al., 2019b, 2019c) and/or the Beishan Orogen along the southern margin of the North China Craton (e.g., Xiao et al., 2003; Wang et al., 2016; Wu et al., 2017b).

Our two Triassic samples and one Cretaceous sample show renewed signals of significant Paleoproterozoic zircon ages of ca. 2500 and ca. 1800 Ma, when compared to Carboniferous-Permian samples (Figs. 8B–E), suggesting the granites from the early Paleozoic Qilian arc were gradually eroded away or were overwhelmed by Proterozoic basement ages. In this sense, Paleozoic arc rocks were less prevalent on the exposed Earth's surface and instead, Proterozoic basement ages became most prevalent in the detrital zircon age spectra. Alternatively, there was a significant reorganization of the drainage systems. Although the source regions for the Cretaceous sample were generally similar to those of the Triassic sedimentary rocks, the Cretaceous paleogeography must have been largely stable as proved by similar detrital zircon age distributions and consistent paleocurrent patterns between the Lower Cretaceous and Oligocene samples in the Yumen Basin, north of Qilian Shan (Wang et al., 2016; Cheng et al., 2019c).

5.2. *Configuration and pre-Cenozoic tectonic evolution of the northern Qilian Orogen*

Detrital zircon age spectra and magmatism timing constraints presented in this study and other published datasets from the northern Qilian Orogen reveal five major age populations at 2550–2350, 1850–1750, 1050–950, 500–435, and 320–240 Ma (Fig. 8). Here, we discuss the importance of these major age signals, and how they constrain the tectonic evolution and paleogeography of the northern Qilian Orogen.

In the Mesoproterozoic, the Tarim (paleo-Qilian) Ocean bounded the southern margin of the contiguous linked Tarim–North China continent

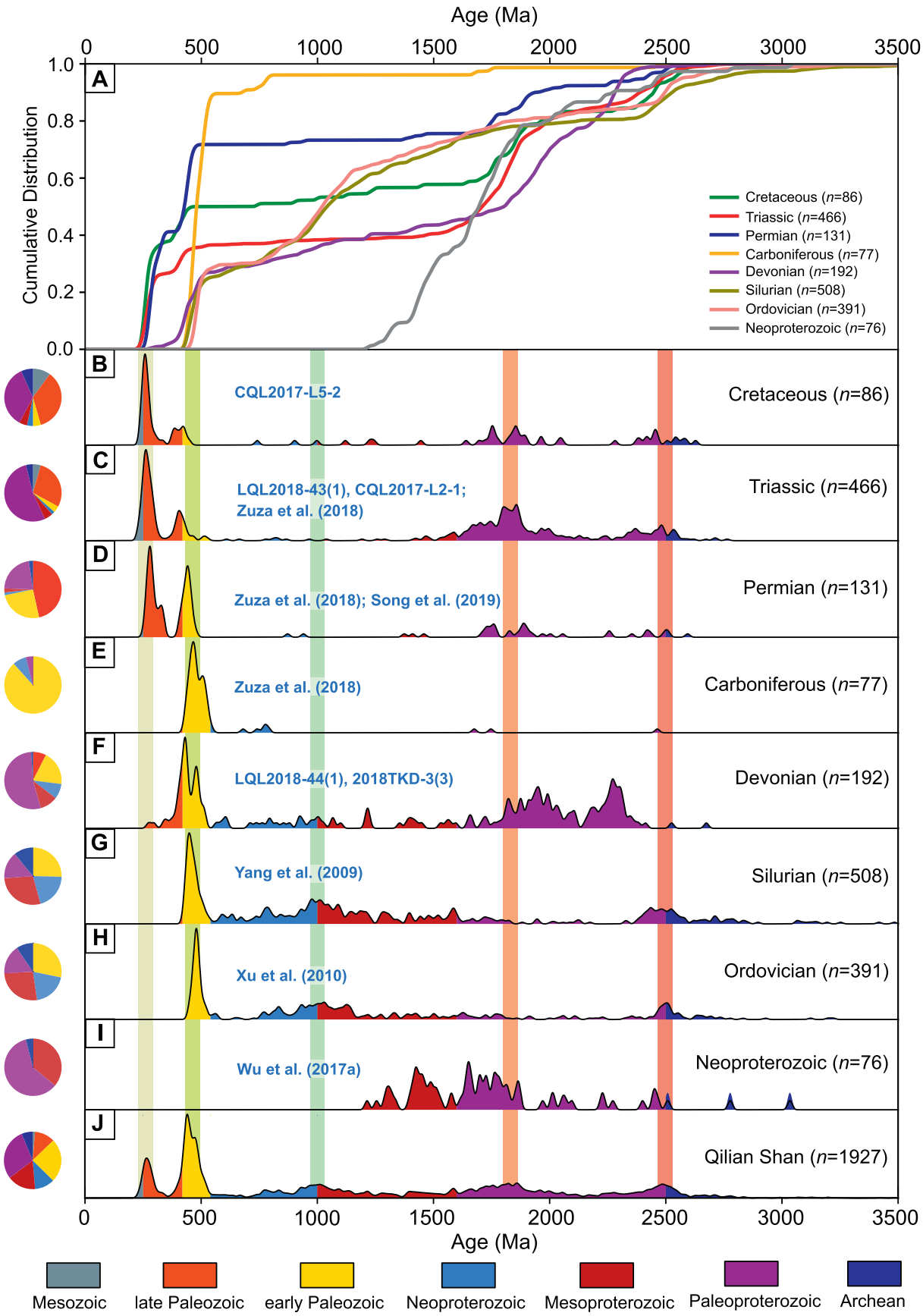

Fig. 8. Detrital zircon U–Pb ages cumulative distribution plot (A) and synthetic relative probability plots (B–J) of the northern Qilian Orogen. Data are from this study, Yang et al. (2009), Xu et al. (2010a), Wu et al. (2017a), Zuza et al. (2018), and Song et al. (2019).

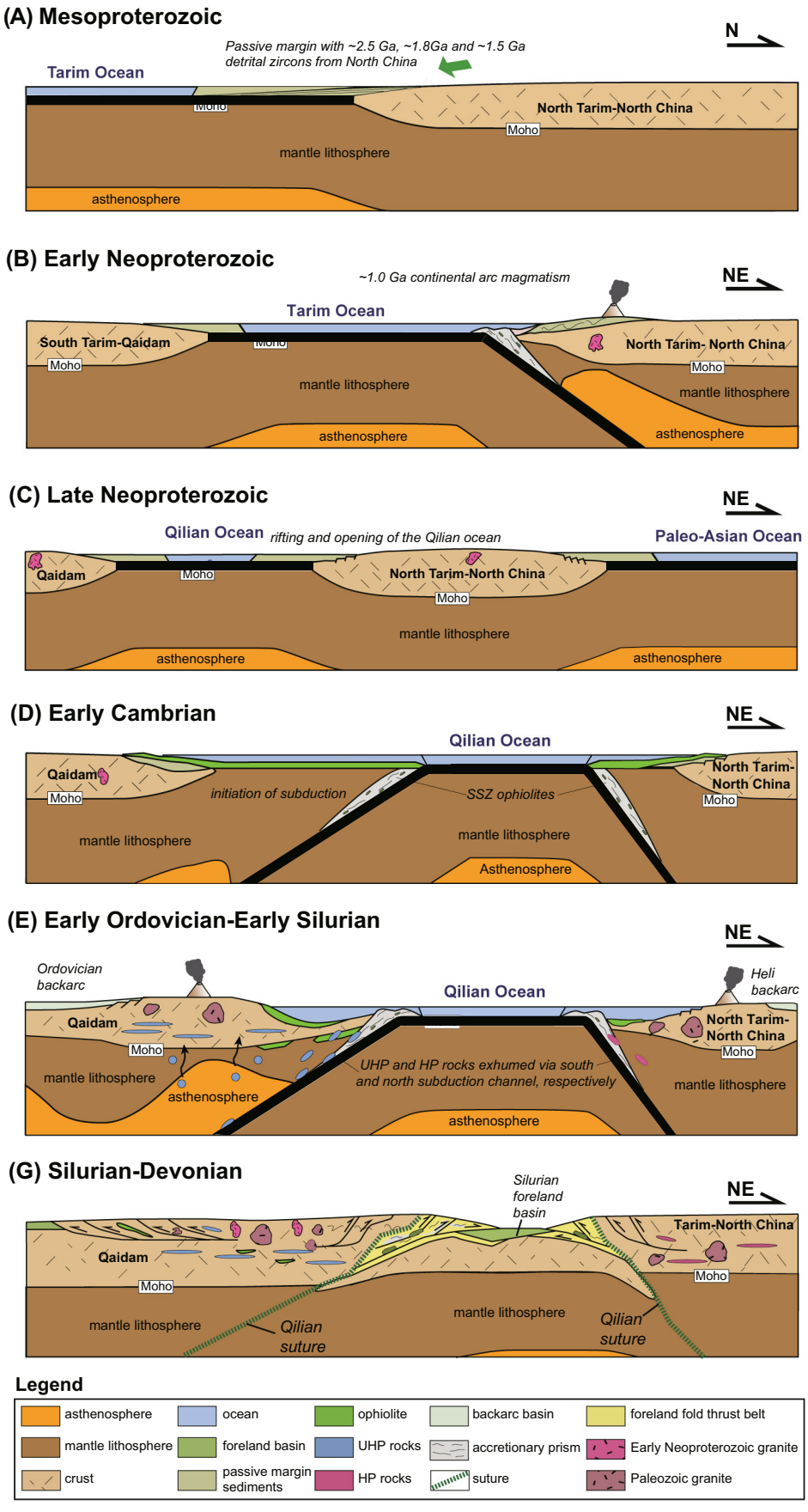

Fig. 9. Models showing the origin and tectonic history of the Qilian Orogen from the Mesoproterozoic through Devonian. (A) Cratonic and/or passive-margin sedimentation along the southern margin of a combined Tarim–North China continent recorded by ca. 2.5, ca. 1.8, and ca. 1.5 Ga detrital zircons through the Mesoproterozoic. (B) North-dipping subduction accommodates the convergence of the Qaidam and Tarim-North China continents during Early Neoproterozoic, leading to the development of the Tarim arc (with ca. 1.0–0.9 Ga magmatism). (C) Late Neoproterozoic to Cambrian rifting opened the Qilian Ocean. Bilateral volcanism (ca. 830–600 Ma) occurs throughout Qaidam, Tarim, and North China. (D) Early Cambrian subduction initiation and generating of suprasubduction zone (SSZ) type ophiolites occurred along the margin of Qaidam and Tarim–North China continents resulting in bivergent subduction. (E) Arc magmatism initiates since early Ordovician to early Silurian, and continental crust was brought to ultrahigh-pressure (UHP) and high-pressure (HP) depths along the subduction channel. (F) Continental collision between Qaidam and North China occurs in early Silurian (ca. 440 Ma) with an intracontinental magmatic activity. Continued convergence variably thrusts basement rocks and ophiolites to surface by the Devonian (modified from Zuza et al., 2018; Chen et al., 2019a).

(Fig. 9A; Zuza and Yin, 2017). Sedimentation along the southern continental passive margin included ca. 2.5, ca. 1.8 and ca. 1.5 Ga zircon grains might be derived from the North China Craton, as supported by the detrital zircon data in Gehrels et al. (2003a), Wu et al. (2017a), Liu et al. (2018a), Zuza et al. (2018) and this study. The Late Neoarchean (ca. 2.5 Ga) is one of the most important periods of continental growth in the North China Craton with extensive magmatism (Polat et al., 2005; Kusky et al., 2007, Kusky et al., 2016; Wan et al., 2015). Late Neoarchean rocks were overlain by dominantly ca. 1.8 and ca. 1.5 Ga strata deposited during post-orogenic extension and magmatism, respectively (e.g., Liu et al., 2006; Kusky et al., 2007; Fan et al., 2014). The ca. 1.0 Ga age population captured from the detrital zircon data (Fig. 8) indicated the protracted early Neoproterozoic granitoid plutons developed as the continental arc along the southern margin of the North China Craton during the enigmatic closure of the Tarim Ocean (Fig. 9B; Guo et al., 2005; Xu et al., 2013; Wu et al., 2016; Zuza et al., 2018).

After this early Neoproterozoic collisional event, possibly associated with Rodinia supercontinent assembly (Zuza and Yin, 2017; Wen et al., 2018), the region started rifting. In the late Neoproterozoic, the Qilian Ocean opened during continental breakup between the Qaidam–Kunlun terrane and North China Craton at ca. 820–775 Ma (e.g., Tung et al., 2013; Song et al., 2014; Wu et al., 2017a), with passive continental margin sedimentation (Tseng et al., 2006; Xu et al., 2015) exposed in the northern Qilian Shan (Figs.1B and 2). Cambrian-aged ophiolites are exposed throughout the Qilian Shan (Fig. 2), and most are supra-subduction zone (SSZ) types with zircon ages ranging from 540 to 500 Ma (Fig. 3A; Xia and Song, 2010; Song et al., 2013; Li et al., 2017; Zuza et al., 2018). The exposure of these ophiolite sequences, extensive distribution of arc-related and syn-to-post-collisional granitoids, and observations of subduction-related high- and ultrahigh-pressure metamorphic rocks in the central–southern Qilian Shan and northern Qilian Shan (as further discussed below) reflect bivergent subduction that initiated along the northern margin of the Qaidam–Kunlun terrane and the southern margin of the North China Craton.

A bivergent subduction configuration is supported by the present-day deep structure derived from a recent broad-band magnetotelluric (MT) sounding profile (Fig. 10; Chen et al., 2019a). The most significant features of the MT profile are the widespread distribution of the low-resistance layers (ca. 20–50 Ω m) within the crust and upper mantle beneath northern Tibet (Fig. 10). These layers reach the shallowest depth (ca. 15–30 km) in the northern Qilian Shan–Hexi Corridor transition zone, and gradually deepened and break off at a depth of ca. 80 km below the southern Qilian Shan (Fig. 10A). The resistance value of the lithosphere beneath the Qilian Shan is similar to that of the modern oceanic lithosphere (Naif, 2018). Yin et al. (2017) suggested that mantle lithosphere with a low resistance of ~10–100 Ω m might represent a fossil oceanic slab. Because of the geometries of the low-resistance layers and their spatial position, Chen et al. (2019a) interpreted that these may represent remnants of the subducted Qilian oceanic lithosphere. Based on the regional geologic evolution interpreted in this study (Fig. 9), we support the inferences of Chen et al. (2019a). However, this interpretation implies that the early Paleozoic oceanic slabs imaged by MT data in the crust and upper mantle have not been significantly modified since their emplacement. Below we briefly provide evidence for this assertion.

Mesozoic regional extension across northern Tibet appears to have mostly influenced the upper crust as observed via seismic profiling (Yin et al., 2008a, 2008b; Cheng et al., 2019a) and field observations of small-scale Mesozoic normal faults (e.g., Zuza et al., 2019; Cheng et al., 2019c). Therefore, extension developed local rift basins (e.g., Vincent and Allen, 1999; Chen et al., 2003), but there is no evidence that the

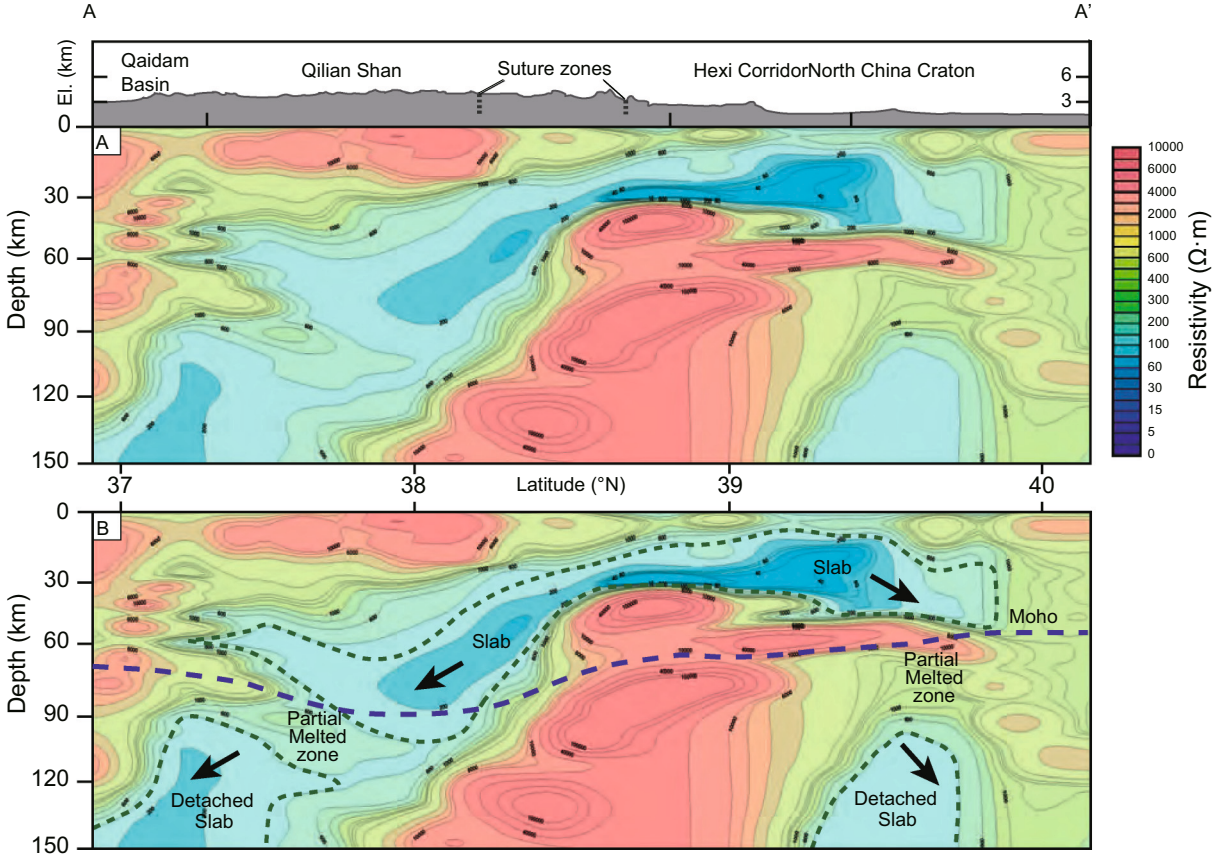

Fig. 10. Inversion profile (A) and tectonic interpretation (B) tectonic interpretation of magnetotelluric sounding profile across the northern Tibetan Plateau (modified from Chen et al., 2019a). Two early Paleozoic suture zone present-day localities are showed on the elevation profile. Moho depth is from Chen et al. (2019a).

crust was greatly thinned. Cenozoic shortening at the northern margin of the Tibetan Plateau was more significant than extension, and could have potentially modified lithospheric geometries. Recent syntheses of Cenozoic shortening across the Qilian Shan demonstrates that it is expressed as dominantly pure-shear shortening mostly south of the suture zones, with southward underthrusting of North China along the paleo-subduction channels (e.g., Zuza et al., 2016, 2018, 2019; Allen et al., 2017; Chen et al., 2019c; Li et al., 2020). With this structural architecture and kinematic framework, crustal deformation was focused in the hanging wall of the crustal-scale ramp that paralleled the south-dipping Qilian suture zone (e.g., Allen et al., 2017; Zuza et al., 2019). Therefore, we argue it is reasonable that the lithosphere underlying, and to the north of, the imaged low-resistivity south-dipping subducting slab may not have been significantly deformed. This interpretation is not unique, but appears viable based on our present understanding of the Qilian Shan. In addition, the top of the interpreted relict slabs almost align with the mapped surface expressions of the sutures (Figs. 1 and 10). The slight offset, with the shallowest low resistance layers located ca. 50 km north of the suture locations, may imply some strain or translation of the lithosphere to disrupt the original alignment between fossil slabs and surface sutures. With these lines of evidence, we support the hypothesis that these low-resistance layers represent remnants of the bivergent subduction of Qilian oceanic lithospheric slabs (Fig. 10B; e.g., Chen et al., 2019a).

Volcanic arc magmatism due to subduction began in the Cambrian, and arc-related intrusions have ages that range from ca. 520 to 440 Ma that are distributed across the Qilian Orogen and north of the Hexi Corridor (Figs. 5A–C; e.g., Wu et al., 2006; Tseng et al., 2009; Wu et al., 2010; Liu et al., 2019; Cui et al., 2017; Zuza et al., 2018; Wang et al., 2020b and this study). Fig. 9D shows subduction initiation, generating SSZ-type ophiolites, and Fig. 9E highlights the mature developed arc in the Ordovician. These arc plutons are part of the central and southern Qilian Shan arc (Fig. S1A) to the south and northern Qilian Shan arc (Fig. S1B) to the north, respectively (Fig. 1B), as evidenced by the zircon U–Pb ages and geochemical data (Fig. 5; Table S1; Tseng et al., 2009; Wu et al., 2010; Cui et al., 2017; Liu et al., 2019; this study). These arc-related magmatic rocks exhibit enriched large ion lithophile elements (e.g., Rb, Ba, Th) and relatively depleted high field strength elements (e.g., Nb, Ta, Ti) patterns with negative Eu anomalies (e.g., Tseng et al., 2009; Cui et al., 2019; Liu et al., 2019), showing arc signatures that may be related to subduction of the Qilian oceanic crust. Syn- and post-collisional granitoids generated by crustal melting during protracted continental collisional orogeny (ca. 440 to 374 Ma; Hu et al., 2005; Wu et al., 2004; Yong et al., 2008; Guo et al., 2015; Wang et al., 2020b) can be interpreted based on compiled discriminant diagrams ((Y + Nb) vs. Rb) from the Qilian Shan (Fig. S1), the granite sample Sample B1139 analyzed in this study (Fig. 5D), and the detrital zircon age signature in Fig. 8 (e.g., Song et al., 2013, Liu et al., 2019; this study).

The subduction process also generated Ordovician ultrahigh-pressure eclogite in northern Qaidam and Silurian high-pressure blueschist in the Qilian Orogen (e.g., Yang et al., 2002; Yin et al., 2007b; Song et al., 2004, 2013, 2014; Menold et al., 2016). Simultaneously, sediments of Silurian turbidite sequences across the Qilian Orogen (e.g., Yang et al., 2009) were deposited in back-arc and forearc-to-foreland basin settings as the Qilian arc transitioned to a collisional orogen (Figs. 8A and 9E). These strata were strongly deformed during the subsequent continental collision (Fig. 3B). This collision led to the provenance shift and restructuring of the drainage systems across the Qilian Orogen.

During the middle-to-late Devonian, extensional orogenic collapse followed, and continental convergence and orogenesis completely ceased by the Carboniferous (e.g., Song et al., 2013; Wu et al., 2016). The primary source rocks changed from containing Proterozoic basement to dominantly early Paleozoic grains from the remnant arc-orogen. Widespread Permian to Triassic shallow-marine sediments were deposited across the Qilian Orogen without significant sedimentary facies variation (Fig. 2). Zircon-age distributions transitioned from early Paleozoic to early Mesozoic ages (Fig. 8). The latter zircon grains were derived from local Permian-Triassic magmatism in the Qilian Shan (Fig. 5E; e.g., Chen et al., 2012; Wu et al., 2016 and this study), arc-volcanic systems associated with the Paleo-Kunlun and Neo-Kunlun arc in the Eastern Kunlun Range, (Figs. 1B and 5E; e.g., Pullen et al., 2008; Cheng et al., 2016b; Wu et al., 2019b, 2019c), and/or the Beishan Orogen (Fig. 1B; e.g., Xiao et al., 2003; Wang et al., 2016).

Jurassic extension rapidly exhumed the basement rocks toward the surface (e.g., Jolivet et al., 2001; Qi et al., 2016; Li et al., 2019), and Jurassic strata were deposited in an intracontinental marine setting with widespread coal deposits (e.g., Lu et al., 2019). Regional extension continued during the Cretaceous (e.g., Chen et al., 2003, 2004; Cheng et al., 2019a; He et al., 2019; Zuza et al., 2019). A local significant pulse of northeast-directed contractional strain overprinted these aforementioned extensional structures, leading to the development of folds and thrusts in the Yumu Shan, northern Qilian Shan, in the early Cretaceous (Chen et al., 2019b). Here Silurian strata were thrust over Cretaceous strata (Fig. 1B; Yang et al., 2007; Zuza et al., 2016; Chen et al., 2019b), which may explain the reheating event documented in low-temperature thermochronology analyses from Cretaceous strata (Li et al., 2020). The late Cretaceous paleogeography was largely stable during the pre-collisional period in the northern Tibetan Plateau (Wang et al., 2016; Cheng et al., 2019c).

5.3. Implications for the Cenozoic development of the northern Tibetan Plateau

The present-day Qilian Shan thrust belt is commonly recognized as the northeastward growth front of the Tibetan Plateau (e.g., Tapponnier et al., 2001; Zheng et al., 2017). Low-temperature thermochronology studies indicate this belt probably experienced multiple pulses of Cenozoic development, including Eocene-Oligocene thrust-dominated deformation (Dupont-Nivet et al., 2004; Clark et al., 2010, 2012; Duvall et al., 2011; Yuan et al., 2013; Qi et al., 2016; Yu et al., 2017; Zhuang et al., 2018; An et al., 2020; Li et al., 2020; Wu et al., 2020) and Miocene mixed-mode of thrusting and strike-slip dominated shortening and exhumation (e.g., Zheng et al., 2006, 2010, 2017; Duvall et al., 2013; Yuan et al., 2013; Zuza et al., 2018; Li et al., 2019; Yu et al., 2019). Deformation-related uplift of the Qilian Shan occurred earlier than the East Kunlun Range to the south, resulting in diachronous construction of the northern of the Tibetan Plateau (Wu et al., 2019a; Bian et al., 2020). This kinematic history since the early Cenozoic requires that plate-boundary stress was transferred rapidly from the India-Asia collisional front across the plateau to the Qilian Shan. Eocene shortening initiation in the Qilian Shan implies that the Hexi Corridor region has remained a stationary northern boundary of the Tibetan Plateau throughout the Cenozoic. Given that the Qilian Shan fold-thrust belt did not progressively propagate northward (e.g., Zheng et al., 2017; Yu et al., 2019), it must have existed as an out-of-sequence thrust belt since the early Cenozoic (e.g., George et al., 2001; Zuza et al., 2019; Li et al., 2020). Here we point out that the MT survey in Fig. 10 reveals that the relict Qilian oceanic lithosphere slab is more or less located below the present-day surface trace of the suture zones that recorded the early Paleozoic Qilian oceanic closure event (Chen et al., 2019a). This observation highlights that the upper crust in the Qilian Shan did not translate northeastward relative to the lower crust and mantle lithosphere. Instead, during progressive shortening deformation and crustal thickening, the upper crust remained in more or less the same position with respect to the entire mantle lithosphere (Fig. 10). This may be interpreted to mean that the northern margin of the Tibetan Plateau was constructed via pure-shearing shortening and thickening (e.g., Simon et al., 2019; Li et al., 2020), accommodated internally within the fold-thrust belt by out-of-sequence deformation.

Numerical modeling demonstrates that the Cenozoic diachronous deformation across the northern Tibet may be controlled by the complex

pre-collisional history that weakened the lithosphere to focus early deformation (Bian et al., 2020). Our detrital zircon dataset combined with other published studies demonstrate that the Qilian Shan consists of a series of early Paleozoic arcs and major suture zones that resulted from oceanic subduction and continental collision (Fig. 8). These orogenic events would have weakened the lithosphere to localize the strain early during Cenozoic orogeny (Bian et al., 2020). Both the Cenozoic Qilian Shan thrust belt and left-slip Haiyuan fault in the northern Tibet geometrically parallel the surface trace of this early Paleozoic collisional belt and resulting suture zone (Taylor and Yin et al., 2009; Zuza et al., 2018). Accordingly, we argue that this relict orogen and suture zone system acted as a mechanical preexisting weakness across the Qilian Shan that was reactivated by the early Cenozoic deformation to establish the northern boundary of the Tibetan Plateau (e.g., Burg et al., 1994; Yin and Harrison, 2000; Zuza et al., 2018). The large-scale south-dipping early Paleozoic fossil oceanic subduction slab (Fig. 8; Chen et al., 2019a) may have facilitated a low-friction basal detachment and/or lithosphere-scale thrust ramp (Zuza et al., 2019) for Cenozoic thrusting. Analog modeling demonstrates that low-friction detachment surfaces in evolving thrust belts lead to very wide thrust systems, with active backthrusts distributed throughout (e.g., Dahlen et al., 1984; Malavieille, 2010). This may explain why the Cenozoic Qilian Shan fold-thrust belt is the widest active thrust belt in the Himalayan-Tibetan Orogen, with active thrusts distributed throughout rather than focused along the frontal thrust systems, like the Main Frontal Thrust in the Himalaya. In summary, we suggest that the pre-Cenozoic tectonic evolution of the Qilian Shan played a decisive role in controlling the pattern, distribution, and sequence of Cenozoic deformation across the northern Tibetan Plateau.

6. Conclusions

In this study, we integrated field observations, U–Pb dating of igneous and detrital zircons, and published datasets to evaluate the pre-Cenozoic tectonic evolution of the Qilian Shan region in northern Tibet. Detrital zircon ages reveal five major age populations that are significant to the history of Qilian Shan: 2550–2350, 1850–1750, 1050–950, 500–435, and 320–240 Ma. The integrated detrital zircon dataset reveals three major depositional shifts and/or variations in drainage patterns that affected sediment provenance in the northern Qilian Shan. Based on observed regional geologic constraints, the timing of local magmatism, and new geophysical observations of the deep structure we propose a coherent tectonic model for the origin and pre-Cenozoic evolution of the northern Qilian Shan. (1) The Tarim Ocean (Paleo-Qilian Ocean), existing between North China-Tarim craton and Qaidam terrane in the early Mesoproterozoic, closed in the early Neoproterozoic, associated with ca. 1.0 Ga magmatism. (2) Late Neoproterozoic to Cambrian rifting opened the Qilian Ocean. (3) Early Cambrian subduction initiation along the margins of the Qaidam and North China-Tarim continents resulted in Cambrian-Ordovician bivergent subduction, arc magmatism, and consumption of the Qilian Ocean. (4) Final ocean closure and continental collision occurred at ca. 440 Ma and was associated with syn- and post-orogenic magmatism. (5) Collisional orogeny variably eroded the basement rocks, reconstructed erosional drainage networks, and altered sedimentary provenance from the early Paleozoic sediments to the late Paleozoic deposits. (6) Mesozoic extension led to the development of thick Jurassic-Cretaceous terrestrial basins with a pulse of early Cretaceous contractional deformation. The pre-Cenozoic tectonic history resulted in preexisting weakness and/or low-friction detachment horizons that played a decisive role in controlling the pattern, distribution, and timing of Cenozoic deformation across northern Tibetan Plateau.

Declaration of Competing Interest

The authors declare that they have no known competing financial interests or personal relationships that could have appeared to influence the work reported in this paper.

Acknowledgments

This research was jointly supported by the China Geological Survey (Nos. DD20190011 and DD20190132), the National Key Research & Development Program of China (No. 2018YFC0603701), the National Natural Science Foundation of China (Nos. 42022029, 41874114 and 41774114) and the Tectonics Program of the National Science Foundation (No. EAR 1914501). Li gratefully thanks financial support from the China Scholarship Council (No. 201808110268) for funding his visit to the University of Nevada, Reno. Constructive reviews and comments by two anonymous reviewers, Dr. Yiduo Liu, Guest Editor Feng Cheng and Editor-in-Chief Thomas J. Algeo greatly improved this manuscript and the clarity of our model. We thank Weicui Ding, Yiping Zhang,Yao-Yao Zhang, Yongchao Wang, Cheng-Guang He, and Xiang Qin for assistance in the fieldwork and U–Pb zircon analysis.

Appendix A. Supplementary data

Supplementary data to this article can be found online at https://doi.org/10.1016/j.palaeo.2020.110091.

References

Allen, M.B., Walters, R.J., Song, S., Saville, C., De Paola, N., Ford, J., Hu, Z., Sun, W., 2017. Partitioning of oblique convergence coupled to the fault locking behavior of fold-and-thrust belts: evidence from the Qilian Shan, northeastern Tibetan Plateau. Tectonics 36 (9), 1679–1698. https://doi.org/10.1002/2017TC004476.

An, K., Lin, X., Wu, L., Yang, R., Chen, H., Cheng, X., Xia, Q., Zhang, F., Ding, W., Gao, S., Li, C., Zhang, Y., 2020. An immediate response to the Indian-Eurasian collision along the northeastern Tibetan Plateau: evidence from apatite fission track analysis in the Kuantan Shan-Hei Shan. Tectonophysics 774 (5), 228278. https://doi.org/10.1016/j.tecto.2019.228278.

Belousova, E., Griffin, W.L., O'reilly, S.Y., Fisher, N., 2002. Igneous zircon: trace element composition as an indicator of source rock type. Contrib. Mineral. Petrol. 143, 602–622.

Bian, S., Gong, J., Chen, L., Zuza, A.V., Chen, H., Lin, X., Cheng, X., Yang, R., 2020. Diachronous uplift in intra-continental orogeny: 2D thermo-mechanical modeling of the India-Asia collision. Tectonophysics 775, 228310. https://doi.org/10.1016/j.tecto.2019.228310.

Bovet, P.M., Ritts, B.D., Gehrels, G., Abbink, A.O., Darby, B., Hourigan, J., 2009. Evidence of Miocene crustal shortening in the North Qilian Shan from Cenozoic stratigraphy of the western Hexi Corridor, Gansu Province, China. Am. J. Sci. 309 (4), 290–329. https://doi.org/10.2475/00.4009.02.

Burchfiel, B.C., Quidong, D., Molnar, P., Royden, L., Yipeng, W., Peizhen, Z., Weiqi, Z., 1989. Intracrustal detachment within zones of continental deformation. Geology 17 (8), 748–752. https://doi.org/10.1130/0091-7613(1989)017<0448:IDWZOC>2.3.CO;2.

Burg, J.P., Davy, P., Martinod, J., 1994. Shortening of analogue models of the continental lithosphere: new hypothesis for the formation of the Tibetan plateau. Tectonics 13 (2), 475–483. https://doi.org/10.1029/93TC02738.

Cawood, P.A., Hawkesworth, C.J., Dhuime, B., 2012. Detrital zircon record and tectonic setting. Geology 40 (10), 875–878. https://doi.org/10.1130/G32945.1.

Chen, X., Yin, A., Gehrels, G.E., Cowgill, E.S., Grove, M., Harrison, T.M., Wang, X.F., 2003. Two phases of Mesozoic north-south extension in the eastern Altyn Tagh range, northern Tibetan Plateau. Tectonics 22, 1053. https://doi.org/10.1029/2001TC001336.

Chen, X., Yin, A., Gehrels, G.E., Cowgill, E.S., Grove, M., Harrison, T.M., Wang, X.F., Yang, N., Liu, J., 2004. Mesozoic N-S extension in the eastern Altyn tagh range on the northern margin of the Qinghai-Tibet plateau. J. Geom. 10 (3), 193–212.

Chen, X., Gehrels, G., Yin, A., Li, L., Jiang, R., 2012. Paleozoic and Mesozoic basement magmatisms of Eastern Qaidam Basin, Northern Qinghai-Tibet Plateau: LA-ICP-MS zircon U-Pb geochronology and its geological significance. Acta Geol. Sin. 86 (2), 350–369. https://doi.org/10.1111/j.1755-6724.2012.00665.x (English Edition).

Chen, X., Shao, Z., Xiong, X., Gao, R., Liu, X., Wang, C., Li, B., Wang, Z., Zhang, Y., 2019a. Fault system, deep structure and tectonic evolution of the Qilian Orogenic Belt, Northwest China. Geol. China (in Chinese with English abstract) 46 (5), 995–1020. doi:10.12029/gc20190504.

Chen, X., Shao, Z., Xiong, X., Gao, R., Xu, S., Zhang, Y., Li, B., Wang, Y., 2019b. Early Cretaceous overthrusting of Yumu mountain and hydrocarbon prospect on the Northern margin of the Qilian orogenic belt. Acta Geosci. Sin. 40 (3), 377–392. https://doi.org/10.3975/cagsb.2019.050901 (in Chinese with English abstract).

Chen, X., Gao, R., Xiong, X., Shao, Z., Li, B., Zhang, Y., 2019c. Deep Seismic Reflection Profiling and Broad-Band Magnetotelluric Sounding of the Qilian Orogenic Belt: Evidence for Bi-Directional Subduction of the Proto-Tethys Ocean plate and Northward Growth of the Qinghai-Tibet Plateau. American Geophysical Union, San Francisco, California. Fall Meeting 2019. (Abstract T22C-03).

Cheng, F., Jolivet, M., Dupont-Nivet, G., Wang, L., Yu, X., Guo, Z., 2015. Lateral extrusion along the Altyn Tagh Fault, Qilian Shan (NE Tibet): insight from a 3D crustal budget. Terra Nova 27 (6), 416–425. https://doi.org/10.1002/2015JB012689.

Cheng, X., Lin, X., Wu, L., Chen, H., Xiao, A., Gong, J., Zhang, F., Yang, S., 2016a. The exhumation history of North Qaidam thrust belt constrained by apatite fission track thermochronology: implication for the evolution of the Tibetan Plateau. Acta Geol. Sin. 90 (3), 870–883. https://doi.org/10.1111/1755-6724.12730 (English Edition).

Cheng, F., Fu, S.T., Jolivet, M., Zhang, C.H., Guo, Z.J., 2016b. Source to sink relation between the Eastern Kunlun Range and the Qaidam Basin, northern Tibetan Plateau, during the Cenozoic. Geol. Soc. Am. Bull. 128 (1/2), 258–283. https://doi.org/10.1130/B31260.1.

Cheng, F., Jolivet, M., Guo, Z., Lu, H., Zhang, B., Li, X., Zhang, D., Zhang, C., Zhang, H., Wang, L., Wang, Z., 2019a. Jurassic–Early Cenozoic tectonic inversion in the Qilian Shan and Qaidam Basin, North Tibet: new insight from seismic reflection, Isopach Mapping, and Drill Core Data. J. Geophys. Res. Solid Earth 124 (11), 12077–12098. https://doi.org/10.1029/2019JB018086.

Cheng, F., Garzione, C.N., Jolivet, M., Guo, Z.T., Zhang, D.W., Zhang, C.H., Zhang, Q.Q., 2019b. Initial deformation of the northern Tibetan Plateau: insights from deposition of the Lulehe Formation in the Qaidam Basin. Tectonics 38. https://doi.org/10.1029/2018TC005214.

Cheng, F., Garzione, C., Jolivet, M., Wang, W., Dong, J., Richter, F., Guo, Z., 2019c. Provenance analysis of the Yumen Basin and northern Qilian Shan: implications for the pre-collisional paleogeography in the NE Tibetan plateau and eastern termination of Altyn Tagh fault. Gondwana Res. 65, 156–171. https://doi.org/10.1016/j.gr.2018.08.009.

Clark, M.K., Farley, K.A., Zheng, D., Wang, Z., Duvall, A.R., 2010. Early Cenozoic faulting of the northern Tibetan Plateau margin from apatite (U-Th)/He ages. Earth Planet. Sci. Lett. 296 (1–2), 78–88. https://doi.org/10.1016/j.epsl.2010.04.051.

Cowgill, E., Yin, A., Feng, W.X., Qing, Z., 2000. Is the North Altyn fault part of a strike-slip duplex along the Altyn Tagh fault system? Geology 28 (3), 255–258. https://doi.org/10.1130/0091-7613(2000)28<255:ITNAFP>2.0.CO;2.

Cowgill, E., Yin, A., Harrison, T.M., Wang, X.F., 2003. Reconstruction of the Altyn Tagh fault based on U-Pb geochronology: role of back thrusts, mantle sutures, and heterogeneous crustal strength in forming the Tibetan Plateau. J. Geophys. Res. Solid Earth 108 (B7), 2346. https://doi.org/10.1029/2002JB002080.

Cui, J., Tian, L., Sun, J., Yang, C., Li, S., 2019. Geochronology and geochemistry of early Paleozoic intrusive rocks in the Lajishan area of the eastern south Qilian belt, Tibetan Plateau: implications for the tectonic evolution of south Qilian. Geol. J. 54, 3404–3420. https://doi.org/10.1002/gj.3327.

Dahlen, F., Suppe, J., Davis, D., 1984. Mechanics of fold-and-thrust belts and accretionary wedges: cohesive coulomb theory. J. Geophys. Res. 89 (B12), 10087–10101. https://doi.org/10.1029/JB089iB12p10087.

Dang, J., 2011. Geochemical characteristics and tectonic implications of Jinfosi granite in north Qilian. Gansu Geol. 20, 40–44.

Davis, W.J., 1997. U-Pb zircon and rutile ages from granulite xenoliths in the Slave province: evidence for mafic magmatism in the lower crust coincident with Proterozoic dike swarms. Geology 25 (4), 343–346. https://doi.org/10.1130/0091-7613(1997)025<0343:UPZARA>2.3.CO;2.

Dickinson, W.R., Gehrels, G.E., 2009. Use of U–Pb ages of detrital zircons to infer maximum depositional ages of strata: a test against a Colorado Plateau Mesozoic database. Earth Planet. Sci. Lett. 288 (1-2), 115–125. https://doi.org/10.1016/j.epsl.2009.09.013.

Du, Y., Wang, J., Han, X., Shi, G.R., 2003. From flysch to molasse-sedimentary and tectonic evolution of late Caledonian–early Hercynian foreland basin in North Qilian Mountains. J. China Univ. Geosci. 14 (1), 1–7.

Dupont-Nivet, G., Horton, B.K., Butler, R.F., Wang, J., Zhou, J., Waanders, G.L., 2004. Paleogene clockwise tectonic rotation of the Xining-Lanzhou region, northeastern Tibetan Plateau. J. Geophys. Res. Solid Earth 109, B04401. https://doi.org/10.1029/2003JB002620.

Duvall, A.R., Clark, M.K., van der Pluijm, B.A., Li, C., 2011. Direct dating of Eocene reverse faulting in northeastern Tibet using Ar-dating of fault clays and low-temperature thermochronometry. Earth Planet. Sci. Lett. 304 (3–4), 520–526. https://doi.org/10.1016/j.epsl.2011.02.028.

Duvall, A.R., Clark, M.K., Kirby, E., Farley, K.A., Craddock, W.H., Li, C., Yuan, D.Y., 2013. Low-temperature thermochronometry along the Kunlun and Haiyuan faults, NE Tibetan Plateau: evidence for kinematic change during late-stage orogenesis. Tectonics 32 (5), 1190–1211. https://doi.org/10.1002/tect.20072.

England, P., Houseman, G., 1989. Extension during continental convergence, with application to the Tibetan Plateau. J. Geophys. Res. Solid Earth 94 (B12), 17561–17579. https://doi.org/10.1029/JB094iB12p17561.

Fan, H.R., Hu, F.F., Yang, K.F., Pirajno, F., Liu, X., Wang, K.Y., 2014. Integrated U–Pb and Sm–Nd geochronology for a REE-rich carbonatite dyke at the giant Bayan Obo REE deposit, Northern China. Ore Geol. Rev. 63, 510–519. https://doi.org/10.1016/j.oregeorev.2014.03.005.

Fedo, C.M., Sircombe, K.N., Rainbird, R.H., 2003. Detrital zircon analysis of the sedimentary record. Rev. Mineral. Geochem. 53 (1), 277–303. https://doi.org/10.2113/0530277.

Gao, R., Wang, H., Yin, A., Dong, S., Kuang, Z., Zuza, A.V., Li, W., Xiong, X., 2013. Tectonic development of the northeastern Tibetan Plateau as constrained by high-resolution deep seismic-reflection data. Lithosphere 5 (6), 555–574. https://doi.org/10.1130/L293.1.

Gehrels, G., Kapp, P., DeCelles, P., Pullen, A., Blakey, R., Weislogel, A., Ding, L., Guynn, J., Martin, A., McQuarrie, N., Yin, A., 2011. Detrital zircon geochronology of pre-tertiary strata in the Tibetan-Himalayan orogen. Tectonics 30 (5). https://doi.org/10.1029/2011TC002868.

Gehrels, G.E., Yin, A., Wang, X.F., 2003a. Detrital-zircon geochronology of the northeastern Tibetan plateau. Geol. Soc. Am. Bull. 115 (7), 881–896. https://doi.org/10.1130/0016-7606(2003)115<0881:DGOTNT>2.0.CO;2.

Gehrels, G.E., Yin, A., Wang, X.F., 2003b. Magmatic history of the Altyn Tagh, Nan Shan, and Qilian Shan region of western China. J. Geophys. Res. 108, 2423. https://doi.org/10.1029/2002JB001876.

Geng, J., Li, H., Zhang, J., Zhou, H., Li, H., 2011. Zircon Hf isotope analysis by means of LA-MC-ICP-MS. Geol. Bull. China 30 (10), 1508–1513.

George, A.D., Marshallsea, S.J., Wyrwoll, K.H., Jie, C., Yanchou, L., 2001. Miocene cooling in the northern Qilian Shan, northeastern margin of the Tibetan Plateau, revealed by apatite fission-track and vitrinite-reflectance analysis. Geology 29 (10), 939–942. https://doi.org/10.1130/0091-7613(2001)029<0939:MCITNQ>2.0.CO;2.

Gong, J.H., Zhang, J.X., Yu, S.Y., 2011. The origin of Longshoushan Group and associated rocks in the southern part of the Alxa block: constraint from LAICP-MS U-Pb zircon dating. Acta Petrol. Mineral. 30 (5), 795–818 (In Chinese with English abstract).

Guo, Z.J., Yin, A., Robinson, A., Jia, C.Z., 2005. Geochronology and geochemistry of deep-drill-core samples from the basement of the central Tarim basin. J. Asian Earth Sci. 25 (1), 45–56. https://doi.org/10.1016/j.jseaes.2004.01.016.

He, C., Zhang, Y., Li, J., Li, H., Sun, D., Xiong, J., 2019. Kinematics of the Maxian Mountain Fault, Northeastern Tibetan Plateau: the history of Cretaceous-Cenozoic sedimentary and tectonic deformation. Acta Geosci. Sin. 40 (4), 563–587. https://doi.org/10.3975/cagsb.2018.111901 (In Chinese with English abstract).

He, P., Song, C., Wang, Y., Meng, Q., Chen, L., Yao, L., Huang, S., Feng, W., Chen, S., 2018. Cenozoic deformation history of the Qilian Shan (northeastern Tibetan Plateau) constrained by detrital apatite fission-track thermochronology in the northeastern Qaidam Basin. Tectonophysics 749 (6), 1–11. https://doi.org/10.1016/j.tecto.2018.10.017.

He, S., Wang, H., Chen, J., Xu, X., Zhang, H., Ren, G., Yu, J., 2007. LA-ICP-MS U-Pb zircon geochronology of basic dikes within Maxianshan rock group in the central Qilian orogenic belt and its tectonic implications. J. China Univ. Geosci. 18 (1), 19–29. https://doi.org/10.1016/S1002-0705(07)60015-6.

Heubeck, C., 2001. Assembly of Central Asia during the middle and late Paleozoic. In: Hendrix, M.S., Davis, G.A. (Eds.), Paleozoic and Mesozoic Tectonic Evolution of Central and Eastern Asia: From Continental Assembly to Intracontinental Deformation, 194. Geological Society of America Memoir, pp. 1–22.

Hu, N., Xu, A., Yang, J., 2005. Characteristics and tectonic environment of Zhigoumen pluton in Longshoushan area. J. Earth Sci. Environ. 27, 5–11 (in Chinese with English abstract).

Huang, H., Niu, Y.L., Nowell, G., Zhao, Z.D., Yu, X.H., Mo, X.X., 2015. The nature and history of the Qilian Block in the context of the development of the Greater Tibetan Plateau. Gondwana Res. 28, 209–224. https://doi.org/10.1016/j.gr.2014.02.010.

Jia, L., Wang, C., Shen, Y., Hu, D., Zhao, X., Qi, B., Zhang, Y., Tao, T., 2018. Formation age of the planation surface in Qilian Mountains: evidence from the electron spin resonance (ESR) dating. Quat. Sci. 38 (3), 668–679. https://doi.org/10.11928/j.issn.1001-7410.2018.03.11 (in Chinese with English abstract).

Jolivet, M., Brunel, M., Seward, D., Xu, Z., Yang, J., Roger, F., Tapponnier, P., Malavieille, J., Arnaud, N., Wu, C., 2001. Mesozoic and Cenozoic tectonics of the northern edge of the Tibetan Plateau: fission-track constraints. Tectonophysics 343 (1–2), 111–134. https://doi.org/10.1016/S0040-1951(01)00196-2.

Kusky, T., Li, J., Santosh, M., 2007. The Paleoproterozoic North Hebei orogen: North China craton's collisional suture with the Columbia supercontinent. Gondwana Res. 12 (1-2), 4–28. https://doi.org/10.1016/j.gr.2006.11.012.

Li, B., Hu, D., Chen, X., Zhang, Y., Wu, H., Wang, C., 2017. Age and tectonic setting of the granite porphyry within Youhulugou ophiolite in the suture zone of the the North Qilian Mountain. Geoscience 31 (5), 883–889 (in Chinese with English abstract).

Li, B., Chen, X., Zuza, A.V., Hu, D., Ding, W., Huang, P., Xu, S., 2019. Cenozoic cooling history of the North Qilian Shan, northern Tibetan Plateau, and the initiation of the Haiyuan fault: Constraints from apatite- and zircon-fission track thermochronology. Tectonophysics 751, 101–124. https://doi.org/10.1016/j.tecto.2018.12.005.

Li, B., Zuza, A.V., Chen, X., Hu, D., Shao, Z., Qi, B., Wang, Z.Z., Levy, D.A., Xiong, X., 2020. Cenozoic multi-phase deformation in the Qilian Shan and out-of-sequence development of the northern Tibetan Plateau. Tectonophysics, 228423. https://doi.org/10.1016/j.tecto.2020.228423.

Lin, Y., Zhang, L., Ji, J., Song, S., 2010. $^{40}Ar/^{39}Ar$ age of Jiugequan lawsonite blueschists in northern Qilian Mountains and its petrologic significance. Chin. Sci. Bull. 55, 2021–2027. https://doi.org/10.1007/s11434-010-3239-8.

Liu, C., Wu, C., Zhou, Z., Yan, Z., Jiang, T., Song, Z., Liu, W., Yang, X., Zhang, H., 2018a. U-Pb detrital zircon geochronology from the basement of the Central Qilian Terrane: implications for tectonic evolution of northeastern Tibetan Plateau. Int. J. Earth Sci. 107 (2), 673–686. https://doi.org/10.1007/s00531-017-1522-5.

Liu, C., Wu, C., Song, Z., Liu, W., Zhang, H., 2019. Petrogenesis and tectonic significance of Early Paleozoic magmatism in the northern margin of the Qilian block, northeastern Tibetan Plateau. Lithosphere 11 (3), 365–385. https://doi.org/10.1130/L1047.1.

Liu, S., Zhao, G., Wilde, S.A., Shu, G., Sun, M., Li, Q., Tian, W., Zhang, J., 2006. Th–U–Pb monazite geochronology of the Lüliang and Wutai Complexes: constraints on the tectonothermal evolution of the Trans-North China Orogen. Precambrian Res. 148 (3-4), 205–224. https://doi.org/10.1016/j.precamres.2006.04.003.

Liu, X., Ren, E., Li, B., Du, Y., Gao, D., Ren, Q., Gao, L., 2018b. Geochronology and petrogenesis of Neoproterozoic S-type granites from the Qilian Block, north-west China, and their geological implications. Geol. J. 54 (4), 2364–2381. https://doi.org/10.1002/gj.3301.

Lu, Z., Zhai, G., Zuo, Y., Wang, Q., Fan, D., Tang, S., Hu, D., Liu, H., Wang, T., Zhu, Y., Xiao, R., 2019. The geological process for gas hydrate formation in the Qilian

Mountain permafrost. Pet. Sci. Technol. 37 (13), 1566–1581. https://doi.org/10.1080/10916466.2019.1594283.
Ludwig, K.R., 2003. Isoplot 3.00. Berkeley Geochronology Center, Special Publication, 4 (70 p).
Malavieille, J., 2010. Impact of erosion, sedimentation, and structural heritage on the structure and kinematics of orogenic wedges: analog models and case studies. GSA Today 20 (1), 4–10. https://doi.org/10.1130/GSATG48A.1.
Menold, C.A., Grove, M., Sievers, N.E., Manning, C.E., Yin, A., Young, E.D., Ziegler, K., 2016. Argon, oxygen, and boron isotopic evidence documenting 40ArE accumulation in phengite during water-rich high-pressure subduction metasomatism of continental crust. Earth Planet. Sci. Lett. 446, 56–67. https://doi.org/10.1016/j.epsl.2016.04.010.
Métivier, F., Gaudemer, Y., Tapponnier, P., Meyer, B., 1998. Northeastward growth of the Tibet Plateau deduced from balanced reconstruction of two depositional areas: the Qaidam and Hexi Corridor basins, China. Tectonics 17 (6), 823–842. https://doi.org/10.1029/98TC02764.
Meyer, B., Tapponnier, P., Bourjot, L., Metivier, F., Gaudemer, Y., Peltzer, G., Shunmin, G., Zhitai, C., 1998. Crustal thickening in Gansu-Qinghai, lithospheric mantle subduction, and oblique, strike-slip controlled growth of the Tibet plateau. Geophys. J. Int. 135 (1), 1–47. https://doi.org/10.1046/j.1365-246X.1998.00567.x.
Molnar, P., England, P., Martinod, J., 1993. Mantle dynamics, uplift of the Tibetan Plateau, and the Indian monsoon. Rev. Geophys. 31 (4), 357–396. https://doi.org/10.1029/93RG02030.
Naif, S., 2018. An upper bound on the electrical conductivity of hydrated oceanic mantle at the onset of dehydration melting. Earth Planet. Sci. Lett. 482, 357–366. https://doi.org/10.1016/j.epsl.2017.11.024.
Pan, G., Ding, J., Yao, D., Wang, L., 2004. Geological Map of Qinghai-Xiang (Tibet) Plateau and Adjacent Areas: Chengdu, China, Chengdu Institute of Geology and Mineral Resources, China Geological Survey. Chengdu Cartographic Publishing House (scale 1:1,500,000).
Polat, A., Kusky, T., Li, J., Fryer, B., Kerrich, R., Patrick, K., 2005. Geochemistry of Neoarchean (ca. 2.55–2.50 Ga) volcanic and ophiolitic rocks in the Wutaishan greenstone belt, central orogenic belt, North China craton: implications for geodynamic setting and continental growth. Geol. Soc. Am. Bull. 117 (11-12), 1387–1399. https://doi.org/10.1130/B25724.1.
Pullen, A., Kapp, P., Gehrels, G.E., Vervoort, J.D., Ding, L., 2008. Triassic continental subduction in Central Tibet and Mediterranean-style closure of the Paleo-Tethys Ocean. Geology 36 (5), 351–354. https://doi.org/10.1130/G24435A.1.
Qi, B., Hu, D., Yang, X., Zhang, Y., Tan, C., Zhang, P., Feng, C., 2016. Apatite fission track evidence for the Cretaceous-Cenozoic cooling history of the Qilian Shan (NW China) and for stepwise northeastward growth of the northeastern Tibetan Plateau since early Eocene. J. Asian Earth Sci. 124, 28–41. https://doi.org/10.1016/j.jseaes.2016.04.009.
Qian, Q., Wang, Y.M., Li, H.M., Jia, X.Q., Han, S., Zhang, Q., 1998. Geochemical characteristics and genesis of diorites from Laohushan, Gansu Province. Acta Pet. Sin. 14, 520–528 (in Chinese with English abstract).
Quan, S., Jia, Q., Guo, Z., Wang, W., 2006. Basic characteristics of granitoids related to tungsten mineralization in the Qilian Mountains. Mineral. Deposita 25, 143–146.
Rubatto, D., 2002. Zircon trace element geochemistry: partitioning with garnet and the link between U–Pb ages and metamorphism. Chem. Geol. 184 (1-2), 123–138. https://doi.org/10.1016/S0009-2541(01)00355-2.
Şengör, A.M.C., Natal'in, B.A., 1996. Paleotectonics of Asia: fragments of a synthesis. In: Yin, A., Harrison, T.M. (Eds.), The Tectonics of Asia. Cambridge University Press, New York, pp. 486–640.
Shao, H., Chen, X., Zhang, D., Shao, Z., Li, B., Wang, Z., Zhang, Y., Xu, S., Shi, J., Miao, H., 2019. The Early Cretaceous tectonic deformation stages and detrital zircon U-Pb ages of Pingshanhu Basin in Hexi Corridor. Geol. China 46 (5), 1079–1093. https://doi.org/10.12029/gc20190509 (in Chinese with English abstract).
Sharman, G.R., Sharman, J.P., Sylvester, Z., 2018. detritalPy: A Python-based toolset for visualizing and analysing detrital geo-thermochronologic data. Depositional Rec. 4 (2), 202–215. https://doi.org/10.1002/dep2.45.
Shi, R., Yang, J., Wu, C., 2004. First SHRIMP dating for the formation of the late Sinian Yushigou ophiolite North Qilian Mountains. Acta Geol. Sin. 78, 649–657 (in Chinese with English abstract).
Simon, A., Yin, A., Li, J., Wu, C., Li, X., 2019. Cenozoic development of Eastern Tibet by pure-shear shortening. In: GSA Annual Meeting in Phoenix, Arizona, USA. https://doi.org/10.1130/abs/2019AM-336062.
Sobel, E.R., Arnaud, N., 1999. A possible middle Paleozoic suture in the Altyn Tagh, NW China. Tectonics 18 (1), 64–74. https://doi.org/10.1029/1998TC900023.
Song, S., Niu, Y., Su, L., Xia, X., 2013. Tectonics of the north Qilian orogen, NW China. Gondwana Res. 23 (4), 1378–1401. https://doi.org/10.1016/j.gr.2012.02.004.
Song, S., Niu, Y., Su, L., Zhang, C., Zhang, L., 2014. Continental orogenesis from ocean subduction, continent collision/subduction, to orogen collapse, and orogen recycling: the example of the North Qaidam UHPM belt, NW China. Earth Sci. Rev. 129, 59–84. https://doi.org/10.1016/j.earscirev.2013.11.010.
Song, S., Yang, L., Zhang, Y., Niu, Y., Wang, C., Su, L., Gao, Y., 2017. Qi-Qin accretionary belt in Central China Orogen: accretion by trench jam of oceanic plateau and formation of intra-oceanic arc in the Early Paleozoic Qin-Qi-Kun Ocean. Sci. Bull. 62 (15), 1038. https://doi.org/10.1016/j.scib.2017.07.009.
Song, S., Wu, Z., Yang, L., Su, L., Xia, X., Wang, C., Dong, J., Zhou, C., Bi, H., 2019. Ophiolite belts and evolution of the Proto-Tethys Ocean in the Qilian Orogen. Acta Petrol. Sin. 35 (10), 2948–2970. https://doi.org/10.18654/1000-0569/2019.10.02 (in Chinese with English abstract).
Song, S.G., Zhang, L.F., Niu, Y.L., Song, B., Zhang, G.B., Wang, Q.J., 2004. Zircon U–Pb SHRIMP ages of eclogites from the North Qilian Mountains, NW China and their tectonic implication. Chin. Sci. Bull. 49, 848–852 (In Chinese with English abstract).
Song, S.G., Zhang, L.F., Niu, Y.L., Su, L., Song, B., Liu, D.Y., 2006. Evolution from oceanic subduction to continental collision: a case study of the Northern Tibetan Plateau inferred from geochemical and geochronological data. J. Petrol. 47, 435–455. https://doi.org/10.1093/petrology/egi080.
Song, Z., Liu, W., Zhang, H., Liu, C., Luo, K., Wu, C., 2019b. Detrital Zircon geochronology and its geological significance of upper permian sandstones in Yushigou area of Western Qilian Mountains, China. Geoscience 33 (1), 112–120 (in Chinese with English abstract).
Stampfli, G.M., Hochard, C., Vérard, C., Wilhem, C., 2013. The formation of Pangea. Tectonophysics 593, 1–19. https://doi.org/10.1016/j.tecto.2013.02.037.
Tapponnier, P., Zhiqin, X., Roger, F., Meyer, B., Arnaud, N., Wittlinger, G., Jingsui, Y., 2001. Oblique stepwise rise and growth of the Tibet Plateau. Science 294 (5547), 1671–1677. https://doi.org/10.1126/science.105978.
Tseng, C., Yang, H., Yang, H., Liu, D., Wu, C., Cheng, C., Chen, C., Ker, C., 2009. Continuity of the North Qilian and North Qinling orogenic belts, Central orogenic system of China: evidence from newly discovered Paleozoic adakitic rocks. Gondwana Res. 16, 285–293. https://doi.org/10.1016/j.gr.2009.04.003.
Tseng, C.Y., Yang, H.Y., Yusheng, W., Dunyi, L., Wen, D.J., Lin, T.C., Tung, K.A., 2006. Finding of Neoproterozoic (~775 Ma) magmatism recorded in metamorphic complexes from the North Qilian orogen: Evidence from SHRIMP zircon U-Pb dating. Chin. Sci. Bull. 51 (8), 963–970. https://doi.org/10.1007/s11434-006-0963-1.
Tseng, C.Y., Yang, H.J., Yang, H.Y., Liu, D.Y., Tsai, C.L., Wu, H.Q., Zuo, G.C., 2007. The Dongcaohe ophiolite from the North Qilian Mountains: A fossil oceanic crust of the Paleo-Qilian Ocean. Chin. Sci. Bull. 52, 2390–2401. https://doi.org/10.1007/s11434-007-0300-3.
Tung, K., Yang, H.J., Yang, H.Y., Liu, D., Zhang, J., Wan, Y., Tseng, C.Y., 2007. SHRIMP U-Pb geochronology of the zircons from the Precambrian basement of the Qilian Block and its geological significances. Chin. Sci. Bull. 52 (19), 2687–2701. https://doi:10.1007/s11434-007-0356-0.
Tung, K.A., Yang, H.Y., Liu, D.Y., Zhang, J.X., Yang, H.J., Shau, Y.H., Tseng, C.Y., 2012. The amphibolite-facies metamorphosed mafic rocks from the Maxianshan area, Qilian block, NW China: a record of early Neoproterozoic arc magmatism. J. Asian Earth Sci. 46, 177–189. https://doi.org/10.1016/j.jseaes.2011.12.006.
Tung, K.A., Yang, H.Y., Liu, D.Y., Zhang, J.X., Yang, H.J., Shau, Y.H., Tseng, C.Y., 2013. The Neoproterozoic granitoids from the Qilian block, NW China: evidence for a link between the Qilian and South China blocks. Precambrian Res. 235, 163–189. https://doi.org/10.1016/j.precamres.2013.06.016.
Wan, Y.S., Liu, D.Y., Dong, C.Y., Xie, H.Q., Kröner, A., Ma, M.Z., Liu, S.J., Xie, S.W., Ren, P., 2015. Formation and evolution of Archean continental crust of the North China Craton. In: Precambrian Geology of China. Springer, Berlin, Heidelberg, pp. 59–136. https://doi.org/10.1007/978-3-662-47885-1_2.
Wang, Q.M., Coward, M.P., 1993. The Jiuxi Basin, Hexi Corridor, NW China: foreland structural features and hydrocarbon potential. J. Pet. Geol. 16 (2), 169–182. https://doi.org/10.1111/j.1747-5457.1993.tb00104.x.
Wang, T., Hong, D.W., Jahn, B.M., Tong, Y., Wang, Y.B., Han, B.F., Wang, X.X., 2006. Timing, petrogenesis, and setting of Paleozoic synorogenic intrusions from the Altai Mountains, Northwest China: implications for the tectonic evolution of an accretionary orogen. J. Geol. 114 (6), 735–751. https://doi.org/10.1086/507617.
Wang, W., Zheng, D., Li, C., Wang, Y., Zhang, Z., Pang, J., Wang, Y., Yu, J., Wang, Y., Zheng, W., Zhang, H., 2020a. Cenozoic exhumation of the Qilian Shan in the northeastern Tibetan Plateau: evidence from low-temperature thermochronology. Tectonics, e2019TC005705. https://doi.org/10.1029/2019TC005705.
Wang, Z., Chen, X., Shao, Z., Li, B., Ding, W., Zhang, Y., Wang, Y., Zhang, Y., Xu, S., Qin, X., 2020b. Petrogenesis of the Late Silurian-Early Devonian granites in the Longshoushan-Helishan area, Gansu province, and its tectonic implications for the Early Paleozoic Evolution of the southwestern Alxa Block. Acta Geol. Sin. 94.
Wen, B., Evans, D.A., Wang, C., Li, Y.X., Jing, X., 2018. A positive test for the Greater Tarim Block at the heart of Rodinia: mega-dextral suturing of supercontinent assembly. Geology 46 (8), 687–690. https://doi.org/10.1130/G40254.1.
Wu, C., Yang, J.S., Yang, H.Y., Wooden, J., Shi, R.D., Chen, S.Y., Zheng, Q.G., 2004. Dating of two types of granite from North Qilian, China. Acta Pet. Sin. 20, 425–432 (in Chinese with English abstract).
Wu, C., Yao, S., Zeng, L., Yang, J., Wooden, J., Chen, S., Mazadab, F., 2006. Double subduction of the early Paleozoic North Qilian oceanic plate: evidence from granites in the central segment of North Qilian, NW China. Geol. China 33, 1197–1208 (in Chinese with English abstract).
Wu, C., Xu, X.Y., Gao, Q.M., Li, X.M., Lei, M., Gao, Y.H., Frost, B.R., Wooden, J., 2010. Early Paleozoic granitoid magmatism and tectonic evolution in North Qilian, NW China. Yanshi Xuebao 26, 1027–1044 (in Chinese with English abstract).
Wu, C., Yin, A., Zuza, A.V., Zhang, J., Liu, W., Ding, L., 2016. Pre-Cenozoic geologic history of the central and northern Tibetan Plateau and the role of Wilson cycles in constructing the Tethyan orogenic system. Lithosphere 8 (3), 254–292. https://doi.org/10.1130/L494.1.
Wu, C., Zuza, A.V., Yin, A., Liu, C., Reith, R.C., Zhang, J., Liu, W., Zhou, Z., 2017a. Geochronology and geochemistry of Neoproterozoic granitoids in the central Qilian Shan of northern Tibet: reconstructing the amalgamation processes and tectonic history of Asia. Lithosphere 9 (4), 609–636. https://doi.org/10.1130/L640.1.
Wu, C., Wang, B., Zhou, Z., Wang, G., Zuza, A.V., Liu, C., Jiang, T., Liu, W., Ma, S., 2017b. The relationship between magma and mineralization in Chaobuleng iron polymetallic deposit, Inner Mongolia. Gondwana Res. 45, 228–253. https://doi.org/10.1016/j.gr.2017.02.006.
Wu, C., Liu, C., Fan, S., Zuza, A.V., Ding, L., Liu, W., Ye, B., Yang, S., Zhou, Z., 2019a. Structural analysis and tectonic evolution of the western domain of the Eastern Kunlun Range, northwest Tibet. Geol. Soc. Am. Bull. https://doi.org/10.1130/B35388.1.
Wu, C., Zuza, A.V., Zhou, Z., Yin, A., McRivette, M.V., Chen, X., Ding, L., Geng, J., 2019b. Mesozoic-Cenozoic evolution of the Eastern Kunlun Range, central Tibet, and

implications for basin evolution during the Indo-Asian collision. Lithosphere 11 (4), 524–550. https://doi.org/10.1016/S0040-1951(03)00053-2.
Wu, C., Liu, C., Fan, S., Zuza, A.V., Ding, L., Liu, W., Ye, B., Yang, S., Zhou, Z., 2019c. Structural analysis and tectonic evolution of the western domain of the Eastern Kunlun Range, northwest Tibet. Geol. Soc. Am. Bull. https://doi.org/10.1130/B35388.1.
Wu, C., Li, J., Zuza, A.V., Liu, C., Liu, W., Chen, X., Jiang, T., Li, B., 2020. Cenozoic cooling history and fluvial terrace development of the western domain of the Eastern Kunlun Range, northern Tibet. Palaeogeogr. Palaeoclimatol. Palaeoecol. 560, 109971. https://doi.org/10.1016/j.palaeo.2020.109971.
Wu, H., Feng, Y., Song, S., 1993. Metamorphism and deformation of blueschist belts and their tectonic implications, North Qilian Mountains, China. J. Metamorph. Geol. 11 (4), 523–536. https://doi.org/10.1111/j.1525-1314.1993.tb00169.x.
Xia, X.H., Song, S.G., 2010. Forming age and tectonopetrogeneses of the Jiugequan ophiolite in the North Qilian Mountain, NW China. Chin. Sci. Bull. 55, 1899–1907. https://doi.org/10.1007/s11434-010-3207-3.
Xia, X.H., Song, S., Niu, Y., 2012. Tholeiite-boninite terrane in the North Qilian suture zone: implications for subduction initiation and back-arc basin development. Chem. Geol. 328, 259–277. https://doi.org/10.1016/j.chemgeo.2011.12.001.
Xiao, W., Windley, B.F., Hao, J., Zhai, M., 2003. Accretion leading to collision and the Permian Solonker suture, Inner Mongolia, China: termination of the Central Asian orogenic belt. Tectonics 22 (6), 1069. https://doi.org/10.1029/2002TC001484.
Xiao, W., Windley, B.F., Yong, Y., Yan, Z., Yuan, C., Liu, C., Li, J., 2009. Early Paleozoic to Devonian multiple-accretionary model for the Qilian Shan, NW China. J. Asian Earth Sci. 35 (3-4), 323–333. https://doi.org/10.1016/j.jseaes.2008.10.001.
Xiong, Z., Zhang, H., Zhang, J., 2012. Petrogenesis and tectonic implications of the Maozangsi and Huangyanghe granitic intrusions in Lenglongling area, the eastern part of North Qilian Mountain, NW China. Earth Sci. Front. 19, 214–227.
Xu, Y., Du, Y., Cawood, P.A., Guo, H., Huang, H., An, Z., 2010a. Detrital zircon record of continental collision: assembly of the Qilian Orogen, China. Sediment. Geol. 230 (1-2), 35–45. https://doi.org/10.1016/j.sedgeo.2010.06.020.
Xu, Y., Du, Y., Cawood, P.A., Yang, J., 2010b. Provenance record of a foreland basin: detrital zircon U–Pb ages from Devonian strata in the North Qilian Orogenic Belt, China. Tectonophysics 495, 337–347. https://doi.org/10.1016/j.tecto.2010.10.001.
Xu, Z.Q., He, B.Z., Zhang, C.L., Zhang, J.X., Wang, Z.M., Cai, Z.H., 2013. Tectonic framework and crustal evolution of the Precambrian basement of the Tarim Block in NW China: new geochronological evidence from deep drilling samples. Precambrian Res. 235, 150–162. https://doi.org/10.1016/j.precamres.2013.06.001.
Yan, Z., Xiao, W., Wang, Z., Li, J., 2007. Integrated analyses constraining the provenance of sandstones, mudstones, and conglomerates: a case study, the Laojunshan conglomerate, Qilian orogen, northwest China. Can. J. Earth Sci. 44 (7), 961–986. https://doi.org/10.1139/e07-010.
Yan, Z., Fu, C., Aitchison, J.C., Buckman, S., Niu, M., Cao, B., Sun, Y., Guo, X., Wang, Z., Zhou, R., 2019. Retro-foreland basin development in response to Proto-Tethyan Ocean closure, NE Tibet Plateau. Tectonics. https://doi.org/10.1029/2019TC005560.
Yang, J.H., Du, Y.S., Cawood, P.A., Xu, Y.J., 2009. Silurian collisional suturing onto the southern margin of the North China Craton: detrital zircon geochronology constraints from the Qilian Orogen. Sediment. Geol. 220 (1-2), 95–104. https://doi.org/10.1016/j.sedgeo.2009.07.001.
Yang, J.S., Xu, Z.Q., Zhang, J.X., Song, S.G., Wu, C.L., Shi, R.D., Li, H.B., Brunel, M., 2002. Early Palaeozoic North Qaidam UHP metamorphic belt on the north-eastern Tibetan plateau and a paired subduction model. Terra Nova 14 (5), 397–404. https://doi.org/10.1046/j.1365-3121.2002.00438.x.
Yang, S., Chen, H., Cheng, X., Xiao, A., He, G., Chen, J., Tian, D., 2007. Deformation characteristics and rules of spatial change for the Northern Qilian Shan thrust belt. Earth Sci. Front. 14 (5), 211–221 (In Chinese with English abstract).
Yin, A., 2010. Cenozoic tectonic evolution of Asia: a preliminary synthesis. Tectonophysics 488 (1-4), 293–325. https://doi.org/10.1016/j.tecto.2009.06.002.
Yin, A., Harrison, T., 2000. Geologic evolution of the Himalayan-Tibetan orogeny. Annu. Rev. Earth Planet. Sci. 28, 211–280. https://doi.org/10.1146/annurev.earth.28.1.211.
Yin, A., Rumelhart, P.E., Butler, R., Cowgill, E., Harrison, T.M., Foster, D.A., Ingersoll, R. V., Qing, Z., Xian-Qiang, Z., Xiao-Feng, W., Hanson, A., 2002. Tectonic history of the Altyn Tagh fault system in northern Tibet inferred from Cenozoic sedimentation. Geol. Soc. Am. Bull. 114 (10), 1257–1295. https://doi.org/10.1130/0016-7606(2002)114<1257:THOTAT>2.0.CO;2.
Yin, A., Dang, Y., Zhang, M., McRivette, M., Burgess, W., Chen, X., 2007a. Cenozoic tectonic evolution of Qaidam Basin and its surrounding regions (part 2): wedge tectonics in southern Qaidam Basin and the Eastern Kunlun Range. In: Sears, J.W., Harms, T.A., Evenchick, C.A. (Eds.), Whence the Mountains? Inquiries Into the Evolution of Orogenic Systems: A Volume in Honor of Raymond A. Price, 433. Geological Society of America Special Paper, pp. 369–390. https://doi.org/10.1130/2007.2433 (18).
Yin, A., Manning, C.E., Lovera, O., Menold, C.A., Chen, X., Gehrels, G.E., 2007b. Early Paleozoic tectonic and thermomechanical evolution of ultrahigh-pressure (UHP) metamorphic rocks in the northern Tibetan Plateau, northwest China. Int. Geol. Rev. 49 (8), 681–716. https://doi.org/10.2747/0020-6814.49.8.681.
Yin, A., Dang, Y., Wang, L., Jiang, W., Zhou, S., Chen, X., Gehrels, G.E., McRivette, M.W., 2008a. Cenozoic tectonic evolution of Qaidam Basin and its surrounding regions (part 1): the southern Qilian Shan–Nan Shan thrust belt and northern Qaidam Basin. Geol. Soc. Am. Bull. 120 (7–8), 813–846. https://doi.org/10.1130/B26180.1.
Yin, A., Dang, Y., Zhang, M., Chen, X., McRivette, M.W., 2008b. Cenozoic tectonic evolution of the Qaidam Basin and its surrounding regions (Part 3): structural geology, sedimentation, and regional tectonic reconstruction. Geol. Soc. Am. Bull. 120 (7–8), 847–876. https://doi.org/10.1130/B26232.1.
Yin, Y., Jin, S., Wei, W., Ye, G., Zhang, L., Dong, H., Xie, C., Liang, H., 2017. Lithospheric rheological heterogeneity across an intraplate rift basin (Linfen Basin, North China) constrained from magnetotelluric data: implications for seismicity and rift evolution. Tectonophysics 717, 1–15. https://doi.org/10.1016/j.tecto.2017.07.014.
Yong, Y., Xiao, W., Yuan, C., Yan, Z., Li, J., 2008. Geochronology and geochemistry of Paleozoic granitic plutons from the eastern Central Qilian and their tectonic implications. Acta Petrol. Sin. 24 (4), 855–866 (in Chinese with English abstract).
Yu, J., Pang, J., Wang, Y., Zheng, D., Liu, C., Wang, W., Li, Y., Li, C., Xiao, L., 2019. Mid-Miocene uplift of the northern Qilian Shan as a result of the northward growth of the northern Tibetan Plateau. Geosphere 15 (2), 1–10. https://doi.org/10.1130/GES01520.1.
Yu, X., Guo, Z., Zhang, Q., Cheng, X., Du, W., Wang, Z., Bian, Q., 2017. Denan Depression controlled by northeast-directed Olongbulak thrust zone in northeastern Qaidam Basin: implications for growth of northern Tibetan Plateau. Tectonophysics 717, 116–126. https://doi.org/10.1016/j.tecto.2017.06.017.
Yuan, D., Ge, W., Chen, Z., Li, C., Wang, Z., Zhang, H., Zhang, P., Zheng, D., Zheng, W., Craddock, W.H., Dayem, K.E., Duvall, A.R., Hough, B.G., Lease, R.O., Champagnac, J.D., Burbank, D.W., Clark, M.K., Farley, K.A., Garzione, C.N., Kirby, E., Molnar, P., Roe, G.H., 2013. The growth of northeastern Tibet and its relevance to large-scale continental geodynamics: a review of recent studies. Tectonics 32 (5), 1358–1370. https://doi.org/10.1002/tect.20081.
Yue, Y.J., Graham, S.A., Ritts, B.D., Wooden, J.L., 2005. Detrital zircon provenance evidence for large-scale extrusion along the Altyn Tagh Fault. Tectonophysics 406, 165–178. https://doi.org/10.1016/j.tecto.2005.05.023.
Zheng, D., Zhang, P., Wan, J., Yuan, D., Li, C., Yin, G., Zhang, G., Wang, Z., Wei, M., Chen, J., 2006. Rapid exhumation at ~8 Ma on the Liupan Shan thrust fault from apatite fission-track thermochronology: implications for growth of the northeastern Tibetan Plateau margin. Earth Planet. Sci. Lett. 248 (1-2), 198–208. https://doi.org/10.1016/j.epsl.2006.05.023.
Zheng, D., Clark, M.K., Zhang, P., Zheng, W., Farley, K.A., 2010. Erosion, fault initiation and topographic growth of the North Qilian Shan (northern Tibetan Plateau). Geosphere 6 (6), 937–941. https://doi.org/10.1130/GES00523.1.
Zheng, D., Wang, W., Wan, J., Yuan, D., Liu, C., Zheng, W., Zhang, H., Pang, J., Zhang, P., 2017. Progressive northward growth of the northern Qilian Shan-Hexi Corridor (northeastern Tibet) during the Cenozoic. Lithosphere 9 (3), 408–416. https://doi.org/10.1130/L587.1.
Zhu, D.C., Zhao, Z.D., Niu, Y., Dilek, Y., Hou, Z.Q., Mo, X.X., 2013. The origin and pre-Cenozoic evolution of the Tibetan Plateau. Gondwana Res. 23 (4), 1429–1454. https://doi.org/10.1016/j.gr.2012.02.002.
Zhuang, G., Johnstone, S.A., Hourigan, J.K., Ritts, B.D., Robinson, A., Sobel, E.R., 2018. Understanding the geologic evolution of northern Tibetan Plateau with multiple thermochronometers. Gondwana Res. 58, 195–210. https://doi.org/10.1016/j.gr.2018.02.014.
Zuza, A.V., Yin, A., 2016. Continental deformation accommodated by non-rigid passive bookshelf faulting: an example from the Cenozoic tectonic development of northern Tibet. Tectonophysics 677-678, 227–240. https://doi.org/10.1016/j.tecto.2016.04.007.
Zuza, A.V., Yin, A., 2017. Balkatach hypothesis: a new model for the evolution of the Pacific, Tethyan, and Paleo-Asian oceanic domains. Geosphere 13 (5), 1664–1712. https://doi.org/10.1130/GES01463.1.
Zuza, A.V., Cheng, X., Yin, A., 2016. Testing models of Tibetan Plateau formation with Cenozoic shortening estimates across the Qilian Shan–Nan Shan thrust belt. Geosphere 12 (2), 501–532. https://doi.org/10.1130/GES01254.1.
Zuza, A.V., Wu, C., Reith, R.C., Yin, A., Li, J., Zhang, J., Zhang, Y., Wu, L., Liu, W., 2018. Tectonic evolution of the Qilian Shan: an early Paleozoic orogen reactivated in the Cenozoic. Geol. Soc. Am. Bull. 130 (5–6), 881–925. https://doi.org/10.1130/B31721.1.
Zuza, A.V., Wu, C., Wang, Z., Levy, D.A., Li, B., Xiong, X., Chen, X., 2019. Underthrusting and duplexing beneath the northern Tibetan Plateau and the evolution of the Himalayan-Tibetan orogen. Lithosphere 11 (2), 209–231. https://doi.org/10.1130/L1042.1.